Test and Evaluation Report

Nondestructive Evaluation Validation Center

Project: DTFH61-C-98-00050

Testing and Evaluation of the PERES II Bridge Inspector

August 30, 2002

Prepared For

Federal Highway Administration
Turner Fairbank Highway Research Center
6300 Georgetown Pike
McLean, Virginia 22101

Prepared By

Wiss, Janney, Elstner Associates, Inc.
4165 Shackleford Road, Suite 100
Norcross, GA 30093
(770) 923-9822

Table of Contents

Table of Contents (Continued)

1. Introduction

The HERMES II project was initiated to develop new ground penetrating radar (GPR) technology for bridge deck evaluation. As the name of the project indicates, the HERMES II project follows a research and development effort that originated with a previous project, known as HERMES (High Speed Bridge Roadway Mapping and Evaluation System). The original HERMES project addressed a broad range of technical challenges that evolved from several important goals. The primary goal of the project was to detect delaminations in concrete bridge decks using GPR technology. Additional goals included collecting data at high speeds (up to highway speeds) and developing data visualization and analysis techniques to make GPR data easier to interpret effectively. HERMES II has been developed to address technical issues from the original HERMES project and to achieve new performance objectives specified by its sponsors. HERMES II has been designed, built, delivered and tested through an integrated process that was led by the Federal Highway Administration (FHWA). This process was made possible by a broad base of supporting organizations described in detail in the following section.

1.1 Background for the HERMES II Project

The original HERMES was designed and built by Lawrence Livermore National Laboratory, (LLNL) leveraging their unique capabilities to address the technical challenges that this project presented. Several papers, reports and presentations chronicled the progress of the HERMES project [1, 2, 3, 4, 5] toward achieving these goals. These studies identified significant deficiencies in the HERMES system, but the HERMES project also advanced the state of the art in GPR for bridge deck evaluation. The primary system deficiency was the range resolution of the system, which was not adequate to consistently detect delaminations in the thickness dimension of concrete bridge decks. However, the system did advance capabilities related to integrating high-speed data collection using a large-scale GPR antenna array, three-dimensional data reconstructions, and tomographic data visualization capabilities.

The current HERMES II project was initiated by a group of State sponsors and was facilitated by the FHWA. These States pooled their funds with the FHWA to collectively fund

the development of a second-generation prototype GPR system. LLNL was tasked with designing and building the HERMES II prototype system, known as PERES II, with the goal of significantly improving GPR capabilities in the areas where the original HERMES system was deficient. This report summarizes an initial evaluation of PERES II by the FHWA Nondestructive Evaluation Validation Center (NDEVC).

1.2 Technical Organizations and Their Project Roles

Three organizations have had principal roles in conceptualizing, planning and subsequently carrying out the work plans for developing and testing the PERES II prototype. These organizations include the FHWA, LLNL and a group of 19 State sponsors, (subsequently referred to as Pooled Fund States) that pooled their funds to support the project work. The project was coordinated by the Federal Highway Administration, which organized project meetings, monitored and approved system development and delivery, and carried out a work plan for evaluating performance of the PERES II system. The first HERMES II project meeting was conducted in January 2000 and brought the FHWA, the Pooled Fund States and LLNL together to make important decisions about objectives for funded work. This first meeting also produced two important organizing groups within the project, Lead States and a HERMES II Technical Panel. Lead States were headed by California and also included Minnesota, Missouri, Michigan, Tennessee, Texas, New York and Illinois. These Lead States provided the majority of the funding for system development and also provided important information about their specific bridge deck issues. The eleven other State organizations that provided important funds for the project included Connecticut, Georgia, Kansas, Montana, North Carolina, New England states, New Jersey, Nevada, Ohio, Iowa and Rhode Island. The HERMES II Technical Panel consisted of several representatives from Pooled Fund States and FHWA research engineers charged with monitoring project progress. In addition the Technical Panel monitored progress and provided guidance for the project as milestones were achieved and task definitions were refined. The Technical Panel met three times via video-conference during the project. A fourth meeting of this Technical Panel is planned for the conclusion of the current phase of the project, subsequent to the delivery of this report.

Lawrence Livermore National Laboratory designed, built and delivered the PERES II system based on the needs identified in the first HERMES II meeting. These tasks were carried out with approval from the FHWA at project milestones and the FHWA, in turn, informed the Technical Panel on project progress. As the informed advisory group throughout the project, the HERMES II Technical Panel was charged with representing the interests of all of the Pooled Funds States involved in the project. An initial evaluation of PERES II performance was carried out by the FHWA NDEVC to provide pooled fund states and other interested parties with an independent assessment of system performance. This performance testing was carried out over controlled test specimens and four field bridge decks. PERES II data from lab and field-testing was processed and is presented in this report to provide a basis for evaluating the system and the overall project.

1.3 Goals of the PERES II Prototype

Goals for PERES II prototype performance were established at the first HERMES II project meeting in January 2000. These goals were developed collectively by the Pooled Fund States and reflect the performance parameters of an instrument that could be relied on in the field. Three specific performance goals were established:

1. Detect defects, at elevations from the top reinforcing steel mat to the deck mid-section, with a reliability of 90 percent through asphalt and concrete overlays.
2. Image delaminations in a bridge with a concrete or asphalt overlay with a spatial accuracy equal to the accuracy of the chain drag method applied on a bare concrete deck.
3. Detect defects at the elevation of the bottom reinforcing steel mat.

NDEVC resources were used to conduct a field and laboratory test program that evaluated the system against these goals as closely as possible.

1.4 PERES II Prototype Configuration

The configuration of the PERES II prototype provides a logical technical approach to addressing the needs identified in Section 1.3. In addition, knowledge gained through experiences reported on in the original HERMES project [4] has been applied to the practical and technical design of the new system. A photograph of the new PERES II system is presented in Figure 1.

Figure 1. PERES II cart collecting data on the Van Buren Road Bridge.

The system consists of a precise motion control system, a new antenna and radar system design, a precise calibration and signal conditioning system, and a computer that coordinates and controls the functions of all of these systems. The key components of the system are described in more detail in the PERES II Hardware section of this report.

1.5 PERES II Validation Testing

A series of field trials of PERES II were conducted by the FHWA NDEVC to address the needs specified in Section 1.3. These field trials allowed the performance of PERES II to be

evaluated under rigorous field conditions. Ground truth data were obtained using traditional means, such as coring, chain drag testing, and hammer tap testing as bridge deck configurations and available inspectors allowed. Traffic control, coordinated through VDOT, was utilized.

The bridges that were included in the field trial evaluations were located in the Fredericksburg, Virginia and Dumfries, Virginia areas, including Structure #1948, which crosses the Rappahonnock River, Structure #1945, which crosses Lake Anna, Structure #1011, which crosses Carter's Creek, and Structure #609, which crosses Quantico Creek. These structures are subsequently referred to as the Chatham bridge, Lake Anna bridge, Carter's Creek bridge and Van Buren Road bridge, respectively. These structures were selected based on their condition, traffic control considerations and availability for testing through VDOT. The bridges were also selected because they represent either typical bare concrete bridge decks or typical asphalt overlaid bridge decks.

In addition to this field validation testing, laboratory testing was conducted using several test specimens that simulate bridge deck features PERES II was designed to detect. This laboratory testing included evaluations of specimens specifically designed to simulate concrete bridge deck delaminations.

2. PERES II Hardware

The PERES II cart is a specialized ground penetrating radar system (GPR), consisting of hardware specifically designed for concrete bridge deck inspection and material investigation. The specialized nature of this equipment requires a few fundamental background concepts to be reviewed for those who are not familiar with GPR and it's basic principles. A brief background on these topics is provided in this section, with references for those who are interested in learning more about GPR. Following this brief introduction to ground penetrating radar, the specific hardware that has been integrated into the PERES II cart radar is described. Supporting hardware, such as mechanical assemblies, motion control equipment and the computer that coordinates and controls all PERES II functions is described.

2.1 Description of Radar Systems

GPR systems provide information about subsurface features by taking advantage of the physical characteristics of microwaves. Microwaves are electromagnetic radiation that occurs at frequencies anywhere in the range from 100 MHz to 300 GHz. One of the useful properties of microwaves is that they travel through many dielectric materials. Dielectric materials have electrical properties that lie between conductors and insulators. Concrete is a dielectric material that allows transmission of radar waves. Microwave propagation characteristics vary depending on the properties of the dielectric material. Changes in the velocity of propagation at interfaces between different materials can be observed using equipment that transmits and receives precisely controlled microwave pulses. This is the essential concept of RADAR, which was originally named by combining letters from a concise description of this concept, RAdio Detection And Ranging.

2.1.1 Basic description of GPR

Radar systems transmit and receive microwave pulses to make measurements for a broad range of familiar applications, such as monitoring aircraft positions and velocities [6]. GPR has also been specialized for applications where materials such as concrete, soil and geology are under investigation. GPR technological development has been motivated by geological applications for decades [7] but GPR systems for civil infrastructure investigations of concrete materials have only recently been designed and produced. This progression occurred, in part, because there are fewer technical challenges involved in designing a GPR for deep geological investigations than for a near surface concrete investigation. The reason for these technical challenges can be more easily understood when the basic concepts involved in detecting objects using radar, such as range, range (depth) resolution, plan resolution and clutter are understood. This discussion will serve the purpose of briefly describing these concepts and how the PERES II design addresses the problem of detecting features like concrete delaminations.

A wide range of parameters can be examined to design a radar system [7], but the primary characteristics used to describe a typical system are its range, depth resolution, plan resolution and the clutter in the received signal. These characteristics are dependent on the radar

system design and the materials that the radar pulse will be traveling through. For any GPR system, the range and depth resolution relate to the depth at which a feature can be detected and the size of the feature that can be detected, respectively. For a demanding application like imaging concrete delamination cracking, range that allows the radar to penetrate through the depth of the bridge deck is required and range resolution that allows the cracked surface (only millimeters thick) of the delaminated concrete to be imaged is critically important. The frequency bandwidth is a primary factor that controls both range and range resolution. Radar that operates at high frequencies can typically image smaller features by taking advantage of high range resolution, but cannot penetrate as deep as an otherwise identical system operating at low frequencies. The converse is also true, since a system that operates at low frequencies can only image larger features with its low range resolution but can penetrate deeper into materials. Therefore, PERES II has been designed to operate over a broad frequency bandwidth, to achieve maximum range resolution and, in turn, detect thin concrete delaminations. At the same time, the PERES II radar must penetrate up to 30 cm in depth through a concrete bridge deck. Low frequencies and enough power at the high end of the frequency bandwidth of the broadband, (covering a broad range of frequencies) PERES II radar pulse are required to image these deep features.

These trade-offs exist due to the phenomena that originally produce a radar reflection from a subsurface bridge deck feature. Any interface in the concrete between materials with different dielectric material properties, such as concrete, air or water, will reflect only a portion of a transmitted radar pulse. Conductive metals, such as reinforcing steel, are essentially perfect reflectors. The geometry of the interface, and the size of the features that make up both sides of the interface determine the type of reflection that will occur. Larger features with flat profiles will produce more significant responses, while smaller features with irregular profiles will produce less pronounced, lower magnitude responses or no response. A high resolution system allows smaller features to be imaged. Better range resolution improves this imaging capability in the depth dimension, while better plan resolution improves it in the two dimensions orthogonal to the depth dimension. This corresponds to the plan view dimensions of a bridge deck for PERES II.

Clutter occurs in radar when a pulse reflects between surfaces multiple times or from objects that are not of interest in a given radar application. Minimizing clutter is important for

any radar system, but it is most difficult for systems where the transmitter, receiver and target are in close proximity to each other. GPR of bridge decks is in the category of difficult applications because target features such as cracks and voids can be obscured by clutter from repeated reflections between the radar antenna and the concrete surface or other features that can mask the response. Clutter must be minimized for effective radar imaging and a variety of measures have been taken to minimize its effects in PERES II data.

2.1.2 Synthetic Aperture Radar (SAR)

Raw data collected using the PERES II radar does not represent target features in the familiar, visually appealing way that bridge plans and drawings do. Instead, raw PERES II data displays reflected energy from a broad beamwidth pulsed radar. The beamwidth of the radar is defined by a solid angle that subtends the area the antenna beam covers. This concept of beamwidth is presented in Figure 2.

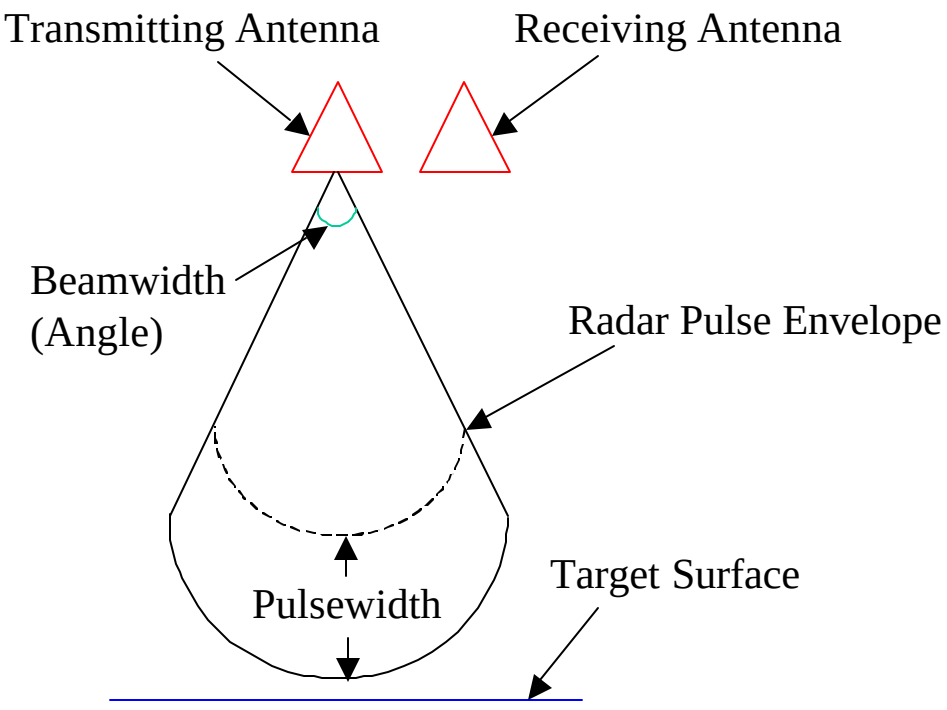

Figure 2. Conceptual drawing of PERES II radar transmitting antenna beamwidth.

Because PERES II has a broad beamwidth, reflected energy returns to the receiving antenna from an individual target when the antenna is in several different locations. Data is collected at many closely and evenly spaced locations when PERES II is used on a bridge deck. When a target feature is centered below an antenna pair, as illustrated by location 1 in Figure 3, the travel time for the reflected energy to reach the antenna is short. This travel time is increased when the antenna is translated to location 2, also shown in Figure 3.

After an individual radar pulse is transmitted, radar waveforms are produced by sampling the reflected radar pulse response at evenly spaced time intervals. When several waveforms are captured at evenly spaced intervals, (for example at positions between location 1 and location 2), it produces a real aperture that allows a response along the interval to be examined. If the real aperture is produced along a linear path, a two dimensional real aperture is created. An image can be constructed from this two-dimensional data (where space is on one axis and time is on the other), which allows the reflected magnitudes of the radar response to be visualized in time and space. This visualization of raw data reveals that reflected energy from individual targets

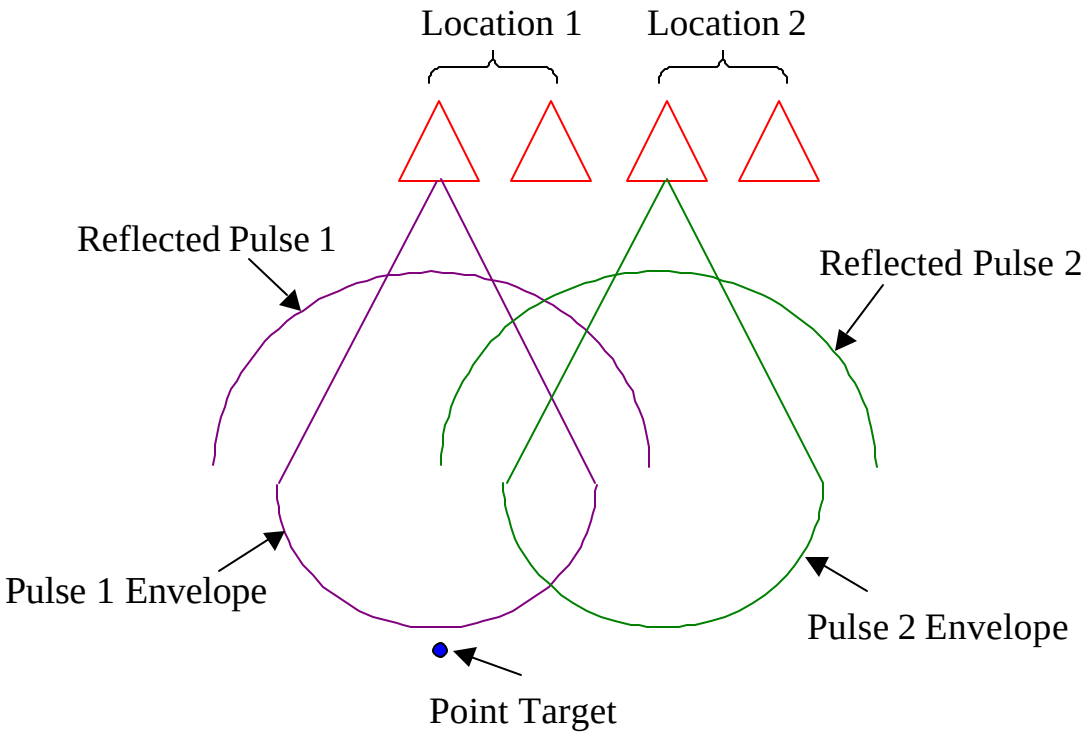

Figure 3. Reflected pulses are captured for a single target feature when the antenna pair is in different locations.

becomes spread out in time and space for raw real aperture radar (RAR) data, which produces images of target features that do not closely resemble the original features. This same type of target feature distortion also occurs if RAR data is collected in three dimensions, as PERES II data is.

To overcome some of the distortions inherent in raw RAR data, an algorithm developed by Jeff Mast [8] can be used to convert raw three dimensional RAR data collected using PERES II to reconstructed synthetic aperture radar (SAR) data that focuses energy back to its reflection sources. The details of this algorithm are not provided here, but the general principles the algorithm operates on can be defined succinctly. In basic terms, the algorithm reconstructs reflection sources by inverting the effects of forward radar propagation for a collection of radar waveforms, (referred to as a wavefield). After this procedure has been performed, many of the difficulties inherent in visualizing radar data can be reduced or eliminated, but some drawbacks still exist. These will be discussed in future sections.

2.1.3 PERES II radar components

PERES II was designed and built using customized components where they were needed and commercially available components whenever possible. The basic components are identified in Figure 4. The system compenents include a motion control and power equipment case; computer, radar and calibration instruments; the radar antenna; a motion control rail; antenna height adjustment rails; and a computer monitor. The PERES II rides on four sets of black, hard rubber wheels. The four sets of wheels are driven by individual stepper motors, while the motion control rail uses a servo motor to move the antenna transverse to the direction of wheel travel. When the system has been set in motion to collect data, it operates in the following sequence. First, the antenna traverses along the rail from the left side of the cart to the right side of the cart. While the antenna traverses, the radar collects data at precisely controlled position intervals that can be set as small as 1 cm. After the antenna reaches the right side of the cart, the wheels move the cart forward at an interval as small as 1 cm. Then, the antenna moves

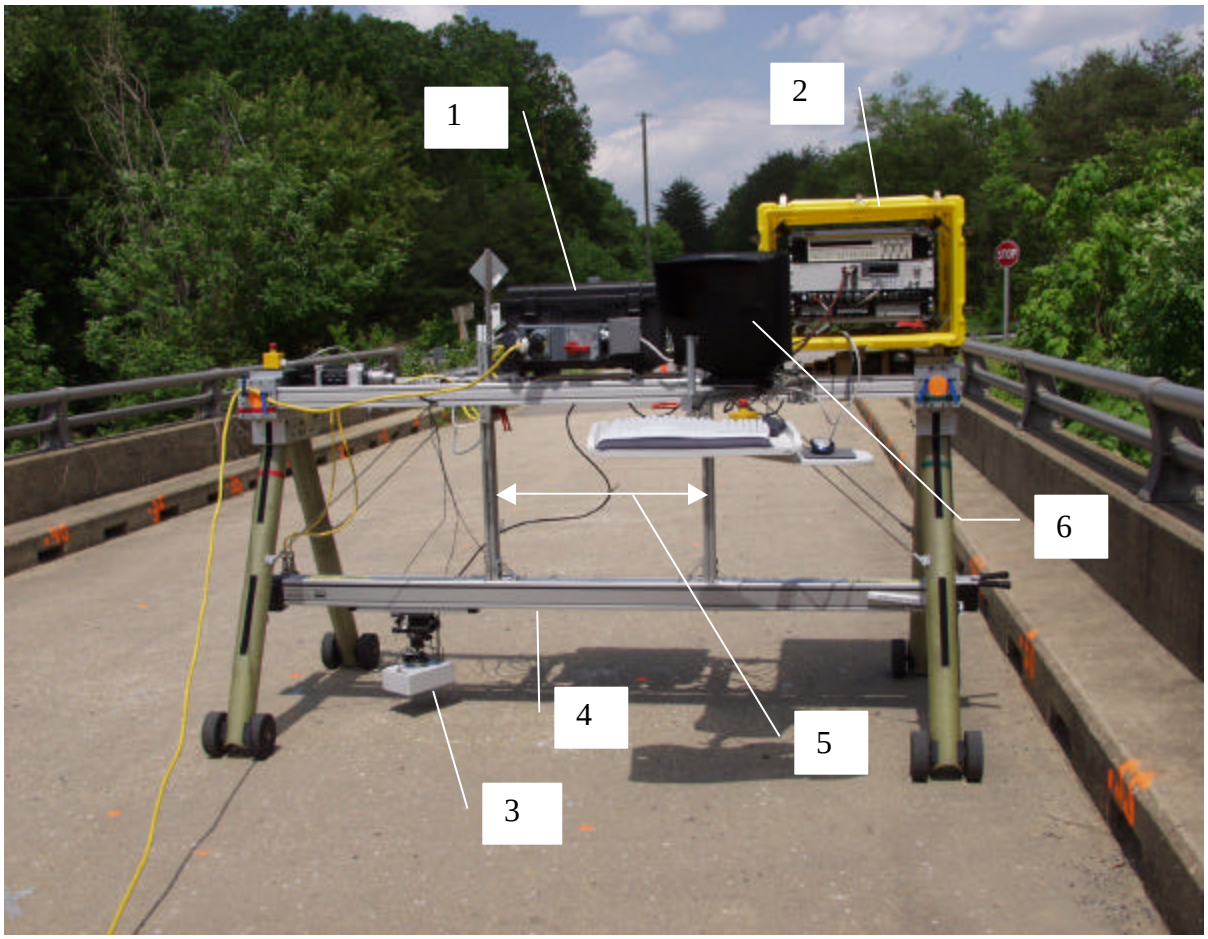

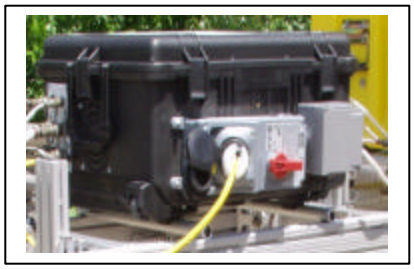

1

2

3

Figure 4. Master image: PERES II cart with labeled components, 1. Motion control and power equipment, 2. PERES II computer, radar and calibration instruments, 3. Radar antenna, 4. Motion control rail, 5. Antenna height adjustment rails, 6. Computer monitor.

from the right side of the cart back to the left side of the cart again while it collects data at the defined interval. This cycle repeats until a specified area has been covered. The height of the antenna can be adjusted before data collection using the hight adjustment rails or a fine adjustment that mounts the antenna to the motion control rail. Power requirements for the entire

system are satisfied by a typical portable generator connected to the system with an extension cord.

2.2 Mechanical assembly

PERES II is designed to be deployed on a bridge deck by assembling many of the compononents on site. This design allows a van to transport the system to the bridge. It also makes the individual components of the system manageable for two people. The assembled system would be too large to fit in a van and moving the assembled system would require additional help. The system requires about half an hour to assemble and half an hour to pack.

2.3 Motion control

System motion control is provided through an integrated, computer controlled system made by Parker-Hannifin's Daedel division. Script files on board the PERES II computer instruct the motion control equipment to move the wheels forward or backward and move the antenna along the rail. The computer controls the coordination of these motions with the radar data collection. The drivers and the master controller for the servo motor and the stepper motors are cooled by fans in the motion control and power equipment case that also serves to protect these components from the elements.

2.4 PERES II computer, radar and calibration instruments

The PERES II computer, radar and calibration instruments are all rack mounted together in a shock resistant yellow case, shown in Figure 4.2. The computer utilizes a 1 GHz processor with 512 MB of RAM running a Linux operating system in a 1U case and also has a read-writable CD-ROM drive, a Zip drive and 3.5 inch disc drive. The computer controls and coordinates all of the operations of the PERES II cart. The radar control instrumentation provides several adjustments for the radar along with input/output connections for the radar antenna. The controls include an analog "offset" dial that adjusts the initial time when the radar begins sampling waveform data and a "span" dial that adjusts the time duration over which each

waveform is sampled. Switches and additional connections on the radar control instrument provide an interface that connects the radar to a calibration timer and a digital gain profile instrument. The calibration timer allows very accurate information about the start and end time of sampled radar waveforms to be recorded for later use in postprocessing data. The digital gain profile instrument provides a means to apply a precise, discrete gain to each data sample in a collected radar waveform. This instrument allows the signal to noise ratio for downsampled data to be improved by maximizing the range that data is sampled over by the computer's analog to digital converter.

3. PERES II Software

PERES II software serves two primary purposes. It provides an interface that includes the computing infrastructure for data collection and it also provides data processing functionality. All of the software has been written to operate in the Linux operating system. The software is written in C and includes a user environment developed at LLNL known as Sigop. Sigop was developed by Jeff Mast at LLNL to facilitate the development of radar applications at their laboratory. PERES II uses programs that run in Sigop as an interface for data collection and a facility for many data visualization and analysis tasks. In addition to satisfying these basic project needs, a unique software tool that runs on internet browser platforms was also developed to supplement data processing documentation. This software tool breaks down data processing tasks with an intuitive user interface that allows these tasks to be completed in a streamlined and efficient manner.

3.1 Data collection software

PERES II data collection tasks are carried out through a graphical user interface in Sigop. This interface allows motion control equipment to be operated with graphical buttons and slider bars on the computer screen that are activated using a mouse. Many of the data collection parameters related to the radar setup, such as data sampling intervals, radar scan coverage area and the physical height of the radar antenna are entered in this interface as well. Before data collection can begin, a timing calibration interface and a digital gain profile interface are both

used to initialize the system. The calibration interface is used to record precisely measured time intervals from signals provided by the PERES II radar. These time measurements allow the radar data sampling interval and the initial radar waveform sample time to be determined, which are both important for subsequent data processing. The digital gain profile interface allows the user to specify the parameters of a gain profile that maximizes the signal to noise ratio of the downsampled data (collected and stored by the PERES II computer). This gain profile is applied to each radar data sample when it is stored. In addition to the improved signal to noise ratio that is achieved with this procedure, typical gain profiles that are generated by PERES II compensate for radar attenuation that reduces the radar response magnitude with increasing depth in the bridge deck. After data files have been collected, they can immediately be reviewed to ensure that the data was collected correctly and contains expected qualitative features.

3.2 Data processing software

Data processing software is crucial for making useful interpretations of PERES II data. PERES II data collected over a bridge deck area can be presented in a raw form, but is generally difficult to visualize and effectively analyze. In fact, this data is collected using the procedure described in Section 2.1.3 and Section 3.1 to make the data compatible with processing routines that produce useful data visualizations from collected raw data (Section 2.1.2). These routines have been developed to produce data reconstructions (Section 2.1.2) which can be examined as tomographic images. These images present subsurface features in a format closely resembling their true geometry and form, within the physical limitations of the method. Algorithms that are used to make reconstruction calculations and supporting algorithms that maximize their effectiveness are described in the following sections. A summary of typical data processing steps is provided in Figure 5. The first three steps in this progression are relatively simple. First, the raw radar data must be collected, as described in Sections 2.1.3 and 3.1. Depending on the objectives of the data processing, the gain profile can be retained or removed. The gain profile would typically be removed to examine the radar response to a bridge deck without any modifications (potentially for a comparison to a calculated model of the GPR response). The gain profile would be retained to visualize the data with the maximum dynamic range possible. After this selection has been made, the background is subtracted from the radar response. This

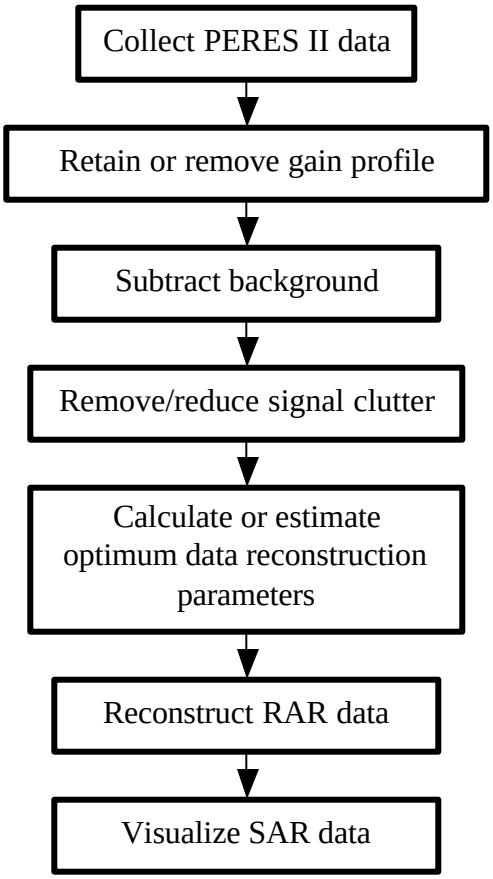

Figure 5. PERES II data processing procedure.

background is the response of the radar without any target objects in its path. This subtraction removes features from the radar data that are not related to the material that the radar is being used to investigate. The remaining processing steps in Figure 5 are addressed in the following sections.

3.2.1 Addressing noise and clutter issues

One of the problems with applying GPR to bridge decks is the close proximity of the radar antenna to the bridge deck target under investigation. The proximity of the target, which includes the top surface and the interior of the concrete bridge deck, to the antenna makes it prone to a phenomenon known generically as signal ringing. While some radar designs are more prone to this phenomenon than others, ringing must be addressed in all radar designs and data

processing schemes. A common method for reducing the ringing response to a feature is to subtract the average response from the entire data set. This method removes features that are always present in PERES II data, such as the top surface of the bridge deck concrete, but allows responses to features that vary with position over the bridge deck, such as reinforcing steel, delamination cracks and voids to stand out. In the laboratory and in the field, this method has proven to be an effective one for removing the effects of signal ringing from PERES II data.

3.2.2 SAR data reconstructions from wavefield backpropagation

Radar data reconstructions that take advantage of SAR techniques (Section 2.1.2) have complicated theoretical underpinnings but understanding how these techniques can be applied to a concrete bridge deck evaluation is basic. Key parameters that these reconstructions require are data or assumptions about the velocity of the radar pulse in concrete and the dispersion characteristics of concrete. Both of these characteristics will vary from one bridge deck to another. If these parameters are known, then a data reconstruction is most effectively realized. If they are not known, then an estimate of these parameters must be made. One of the best means of estimating these parameters is to know the thickness of the bridge deck and to be able to identify the front and back surface of the bridge deck in the radar response. If all of this information is available, then the velocity of the radar pulse in the concrete can be determined and one of the key parameters for producing an accurate reconstruction will be satisfied. Bridge plans are useful for obtaining this kind of information, but a core from a bridge deck is most valuable for estimating the bridge deck thickness, since any overlays or variations from the original bridge design can be observed in the core. Dispersion characteristics of concrete are much more complicated and have to be assumed for the purposes of typical PERES II GPR data processing. Fortunately, dispersion characteristics are not a dominant variable for reconstructions of most PERES II data. Figure 6 presents images from reconstructed test data that was collected at the Van Buren Road Bridge. These images show how estimating velocity parameters and other processing parameters affect data reconstruction results.

All six of the images in Figure 6 were produced using the same data, collected using PERES II on the Van Buren Road Bridge deck. The only differences between these images are

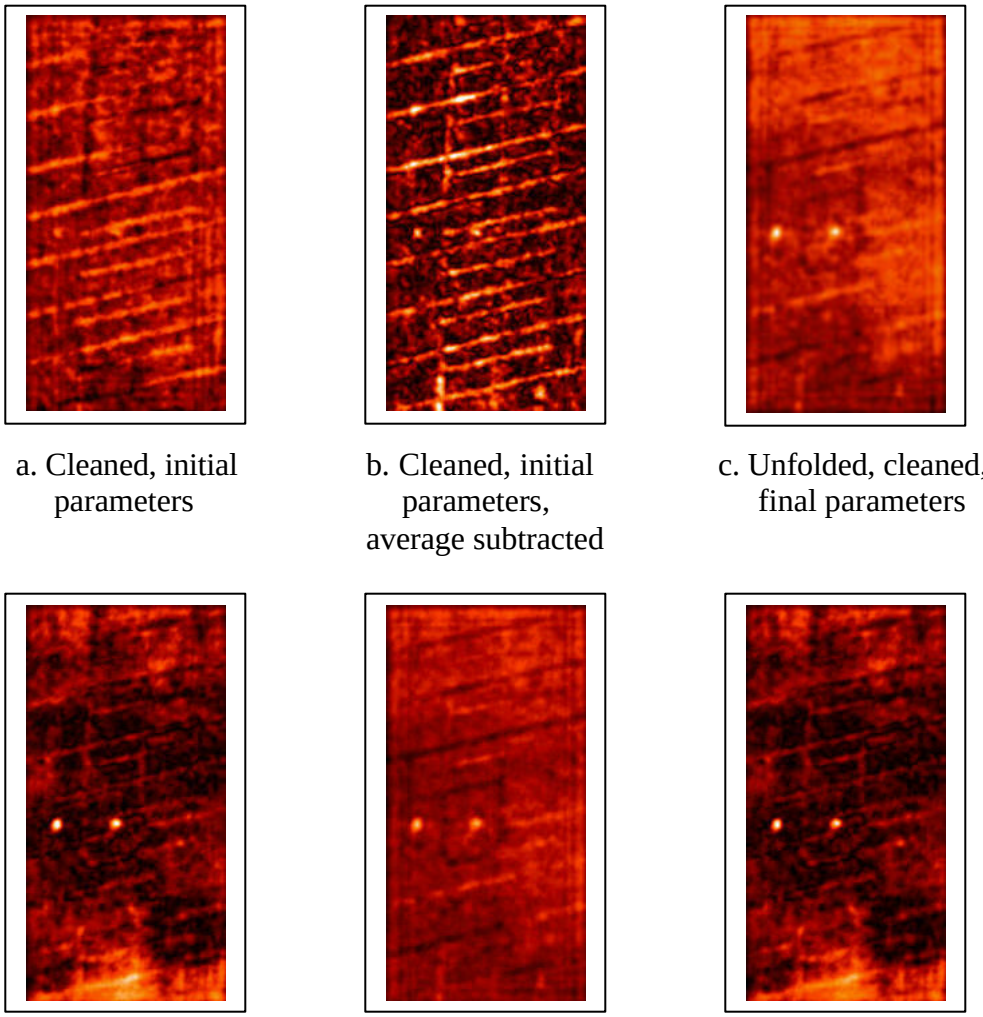

a. Cleaned, initial parameters

b. Cleaned, initial parameters, average subtracted

c. Unfolded, cleaned, final parameters

d. Unfolded, cleaned, final parameters, average subtracted

e. Unfolded, cleaned, initial parameters

f. Unfolded, cleaned, initial parameters, average subtracted

Figure 6. Data reconstruction results for a 3 m x 1.5 m area of the Van Buren Road Bridge deck for a variety of data processing methods.

the methods that were used to process the data. All of the images present reconstructed data from the top mat of reinforcing steel inside the deck. Although useful information can be obtained from all of these images, the image in Figure 6b provides the highest contrast, the most accurate focus and has the fewest indications of clutter. The clear, precise imaging of the reinforcing steel below the deck illustrates the quality of this image. This discussion clarifies how important appropriate processing parameters and procedures are for effective data

interpretation. Appendix A contains a summary of the differences between the methods used to process this data.

3.2.3 Data visualization and analysis

Interpreting PERES II data through visualization and analysis is a unique process because of the high resolution of the system and the accuracy of its data sampling. These unique features are integrated with data processing algorithms that produce exceptional three-dimensional imaging capabilities. For explanation purposes, the most important aspect of these images is the organization of the reconstructed data the system produces. The data is typically visualized by presenting images of tomographic layers, which are analagous to more commonly visualized layers in a computerized axial tomography (CAT) scan for medical purposes. These layers can correspond to plan view sections at varying depths in the bridge deck, as shown in Figure 7.

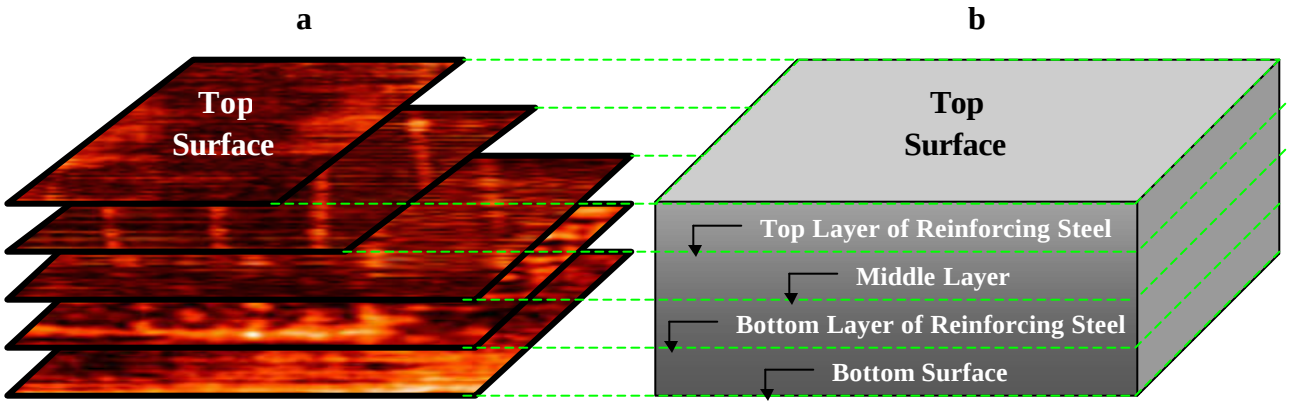

Figure 7. (a) Plan view tomographic layers of PERES II data and (b) schematic of concrete bridge deck layers that are frequently of interest.

As Figure 7 indicates, images can be extracted from the data that correspond to features at specific depths, such as the top layer of reinforcing steel. Typical PERES II data reconstructions produce many tomographic layers, including layers at depths corresponding to features of interest that can be viewed individually. The data presented in this report displays images using a colormap that maps radar response values with low magnitudes from black to dark orange and high magnitude responses from light orange to white. High magnitude responses typically indicate features such as reinforcing steel, delamination and void defects, and

signal clutter. Low magnitude responses typically indicate solid concrete areas. Detailed interpretations of many PERES II images are presented in further sections of this report.

4. Laboratory Validation Testing

Several laboratory specimens were developed for PERES II testing at the NDEVC. These specimens were designed to assess key performance characteristics of the PERES II system. These characteristics included the depth of penetration that the system could image features at, the size of voids that the system could image and the profile of delamination cracking that the system could image. The specimens are described in the following section and selected portions of data sets are presented where they illustrate PERES II response characteristics relevant to bridge deck evaluation.

4.1 Test specimens

PERES II test specimens were produced using a Virginia DOT concrete bridge deck mix design, commonly known as an A4 mix design, Appendix B. The geometry of the specimens is illustrated in Appendix C. Two distinct test specimen designs were used to evaluate delamination detection capabilities of the PERES II system, while three additional test specimen designs were used to evaluate other characteristics of the system. Figures C1 and C2 illustrate the two specimen designs used to evaluate delamination detection capabilities, while Figures C3, C4 and C5 illustrate the remaining specimen designs.

The test specimen design illustrated in Figure C1 is a simplified model of a concrete delamination. This design uses two parallel, flat plates to mimic delamination features with different air gap profiles. Different profiles have larger or smaller gaps between the two plates, as measured in the thickness dimension, between the cover plate and the base plate. PVC pipe spacers, preferable to metals due to their low dielectric contrast with concrete, are used to create the air gap between the parallel plates. Although the surface roughness of these plates is minimal and therefore differs from a real concrete delamination, this simplified model of the delamination produces useful results. Three different cover plates were used in the testing,

illustrating the differences between radar responses to air gaps at 1 in., 2 in. and 3 in. below the surface of the concrete.

The test specimen design illustrated in Figure C2 is a simulation of a concrete delamination that was produced by physically cracking two pieces of concrete in a 1 ft. square area in the middle of the concrete slab, as indicated by the dashed line in the plan view drawing of this specimen. This crack is very similar to a real delamination crack, but the additional feature this specimen offers is the capability to adjust the air gap between the top and bottom portion of the slab. The side view of this specimen illustrates the profile of the simulated crack.

Figure C3 illustrates a specimen designed to determine the depth of penetration that PERES II can achieve in a typical bridge deck. This is accomplished by designing reinforcing steel into the specimen at depths that vary. The strong radar reflection produced by the reinforcing steel clearly indicates whether the radar response is strong enough to be detected at a given depth in the test slab. The specimens in Figures C4 and C5 illustrate the capabilities of the PERES II system for detecting reinforcing steel and voids with different sizes.

4.2 Summary of test results

PERES II performance characteristics were evaluated using data collected from laboratory test specimens that were designed specifically for this evaluation. An initial interpretation of these laboratory performance characteristics is presented in this section. Results from field tests can be interpreted with more confidence when the phenomena observed in this laboratory testing are considered.

Simulated delamination crack features, planar air gaps and void features are all relevant to bridge decks, but test responses to crack features and planar air gaps are particularly important when they are considered in relation to the project goals for PERES II. Therefore, a more detailed summary is dedicated to images and discussion that illustrates responses to these types of features, while other response phenomena are discussed in more general terms.

As referenced previously, Figures C1 and C2 in Appendix C illustrate the parallel plate test specimen design and the simulated delamination crack specimen design, respectively. The results from C1 testing are presented in Figures 8 and 10, where Figure 8 illustrates a typical result from a test where the two flat plates were positioned in a flush configuration such that the

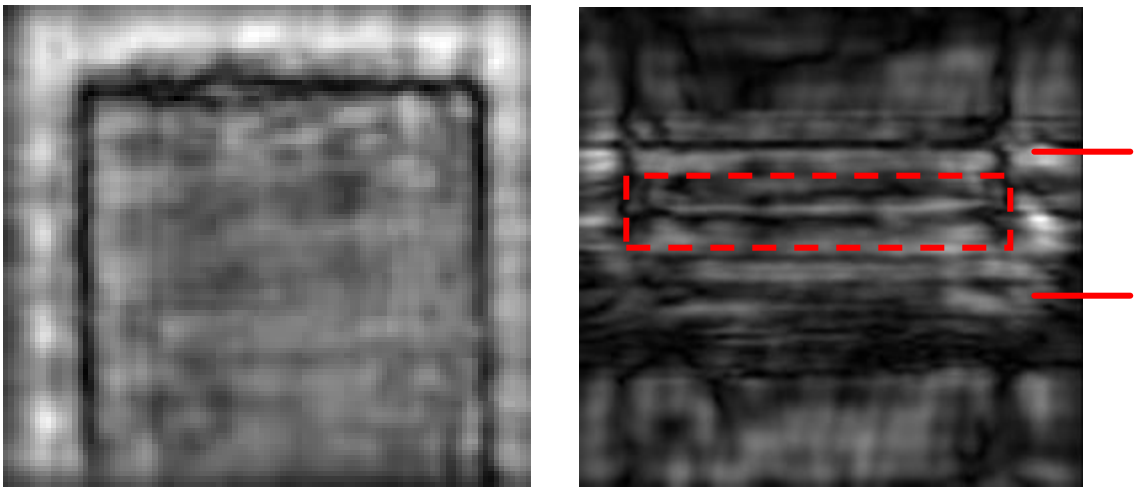

(a) **(b)**

Figure 8. PERES II results from parallel plate slabs in a flush configuration. (a) Plan view image of reconstructed data (b) elevation view of reconstructed data.

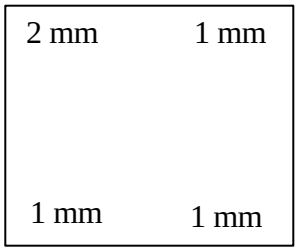

Figure 9. Measured estimate of the air gap between parallel plate slabs in a flush configuration (measured in cm) at each corner of the test specimen.

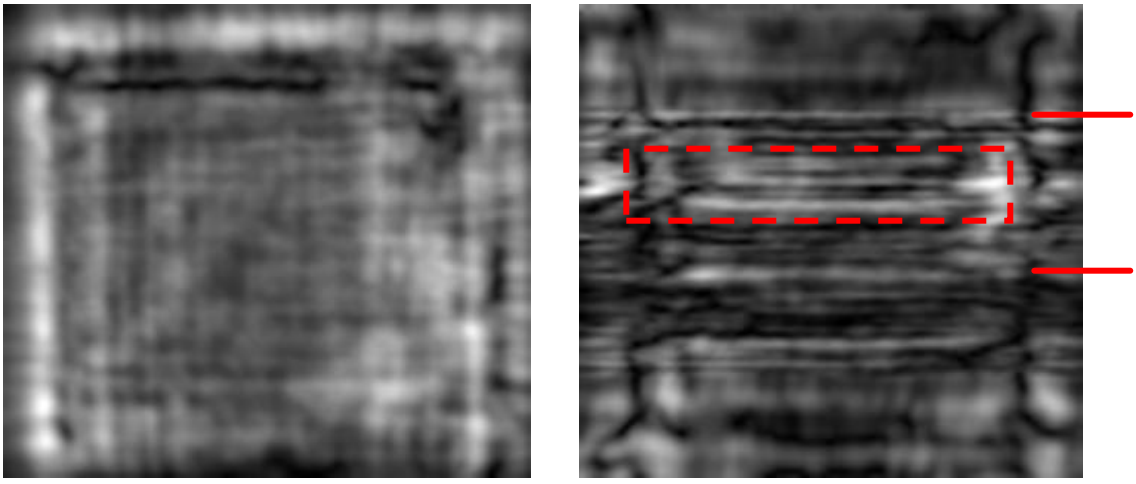

(a) **(b)**

Figure 10. PERES II results from parallel plate slabs with a 0.64 cm air gap. (a) Plan view image of reconstructed data (b) elevation view of reconstructed data.

air gap between the cover plate and the base plate was minimized by positioning the cover plate directly on top of the base plate. The flat plates were not perfectly flush, as indicated in Figure 9. Figure 10 illustrates the same plates in a similar configuration, with an air gap between the two slabs that was 0.64 cm thick. In the testing described here the cover plate is 7.62 cm thick and the base plate is 10.16 cm thick. Figure 8 and 10 data are both sampled from reconstructed data, processed using methods described in Section 2.1.2.

There are several notable features in the reconstructed data from these parallel, flat plate specimens and details can be observed in the plan view format (a) and elevation view format (b). Figures 8 and 10 both present response magnitudes in the reconstructed radar data by plotting grayscale values ranging from black, for low magnitudes, to white, for high magnitudes. Figure 8a features a plan view image layer, sampled from a three-dimensional tomographic data reconstruction at the depth of the interface between the two flat plates. This image indicates the left, right and top boundaries of the plate with a pronounced, dark border that defines three sides of the square specimen in the image. The bottom boundary of the plate can be observed as a darkened border at the bottom edge of the image, but this boundary is only partially imaged. The plate area in Figure 8a displays the magnitude of the reconstructed response from the plate interface. The magnitudes of the responses in this plate area are relatively homogeneous when compared with variations caused by boundaries or other localized features. This response also has a high magnitude when compared with corresponding responses to the plate in image layers above or below it. A response of this type is likely to be indicative of an interface between materials with significantly different dielectric properties, such as concrete and air. The concrete to air interface that exists between the plates is therefore a logical explanation for the observed response.

Figure 8b presents an elevation view of the three-dimensional tomographic data reconstruction. This view of the data allows the interface between the two concrete slabs to be viewed edge on. In this particular image the boundary between the top surface of the concrete cover plate and the air above the concrete is marked by a red hash mark. Below this, a dashed red box identifies the location of the response to the concrete plate interface. In this image, the interface is represented by a horizontal, light colored strip that divides the top and bottom half of the dashed line box.

A metal plate was placed in the interface between the parallel concrete plates in subsequent testing (producing a strong, easily located response) to assure that the location of the interpreted interface was correct. Other potential causes of the observed high magnitude response at the interface were considered, such as signal ringing, but these were eliminated from consideration by further analysis. The bottom of the base plate of this specimen was identified in the image and is denoted by the lower red hash mark.

Figure 10 presents data from the same plate specimens that were imaged in Figure 8, but this time a significant gap (0.64 cm measured in the depth dimension) is introduced between the base plate and the cover plate. As a result, the response in Figure 10b, highlighted by the dashed line box, indicates a pronounced high magnitude response that traverses a horizontal strip across the middle of the box. In addition to this feature, which appears to be a reflection from the top surface of the air gap between the two plates, there is a second high magnitude response indicated by a horizontal strip across the bottom half of the dashed line box. This second response appears to be an image of the bottom surface of the air gap between the two plates. Hash marks denote the top and bottom surface of the pair of stacked concrete plates, similar to the markings in Figure 8. The increased magnitude of the response observed in Figure 10a (relative to Figure 8a) and the changes in the characteristics of the response from figure 8b to 10b indicate the relative sensitivity of the system to air gaps of varying sizes between planar surfaces.

The simulated concrete crack specimen tested using PERES II is illustrated in Figure C2. The plan view drawing of the specimen indicates a cracked area between two concrete slabs using a dashed line. An elevation view drawing illustrates the physical geometry of this specimen and the planar crack when the specimen is configured with a minimum sized air gap between the two halves of the test piece. Shims are used to vary the size of the air gap between the two halves of the cracked specimen.

The same image format described in Figures 8 and 10, is used to illustrate the PERES II response to the simulated crack specimen in Figures 11 and 12. In this case, the area of interest is narrowed to the 30.5 cm square area that corresponds to the crack in the specimen. In Figures 11a and 12a this area is defined by a red, dashed line box. Close observations of the features in these two boxed areas allow several interesting features to be observed. One of the features of interest is near the middle of the dashed line box in Figure 12a. There is a small dark area

(corresponding to a low magnitude response) encircled by a light area (corresponding to a high magnitude response). Moving radially outward, there is another dark band followed by a light band. The interpretation of this response is aided by the knowledge that the profile of the crack between the two halves of this specimen has a domed shape that crowns upward in the middle of the cracked area. Due to the profile of this crown shape, it appears that locations near the middle and near the edges of the cracked area reflect radar energy most effectively.

Because the dashed line boxed areas in Figures 11a and 12a exhibit characteristics that are indicative of the geometry of the crack, a comparison of the features in these two images is useful. One image corresponds to a minimized air gap between cracked surfaces and the other image corresponds to an approximately 0.25 cm open gap. Specifically, the magnitude of the overall response in the dashed line boxed area is increased significantly when the configuration changes from a minimized air gap (Figure 11a) to a more open gap (Figure 12a). These results emphasize the effects of the geometry of a crack on the imaging capability of the system. A crack that is oriented at an oblique angle relative to the bridge deck surface is more difficult to image with radar than a crack that is parallel to the surface, since the obliquely oriented crack reflects a significant proportion of the incident radar pulse away from the receiving antenna. Figures 11b and 12b illustrate the elevation view images of the simulated crack specimen data from PERES II. The dashed line boxed areas indicate locations corresponding to data from the crack location. Although this image is complicated by a variety of edge effects, the relative magnitude of the response in the boxed areas for the minimized air gap (Figure 11b) relative to the more open gap (Figure 12b) is consistent with the plan view observations. As a general note, all of the results from the simulated crack specimen should be viewed in light of the fact that the crack surfaces could not be mated perfectly, even for the minimized air gap configuration. Therefore, some cracks in the field would be expected to present a smaller air gap between crack surfaces than this controlled test was capable of duplicating.

The PERES II response to reinforcing steel, voids, and the size of these features were all considered based on results from specimens C3, C4 and C5. The results from these specimens indicated several important performance characteristics, including a demonstration of the capability of the system to image features as deep as 18 cm below the surface of the concrete (based on PERES II results from specimen C3 illustrated in Figure 13). An example result from specimen C5, presenting PERES II responses to PVC pipe voids, is provided in Figures 14.

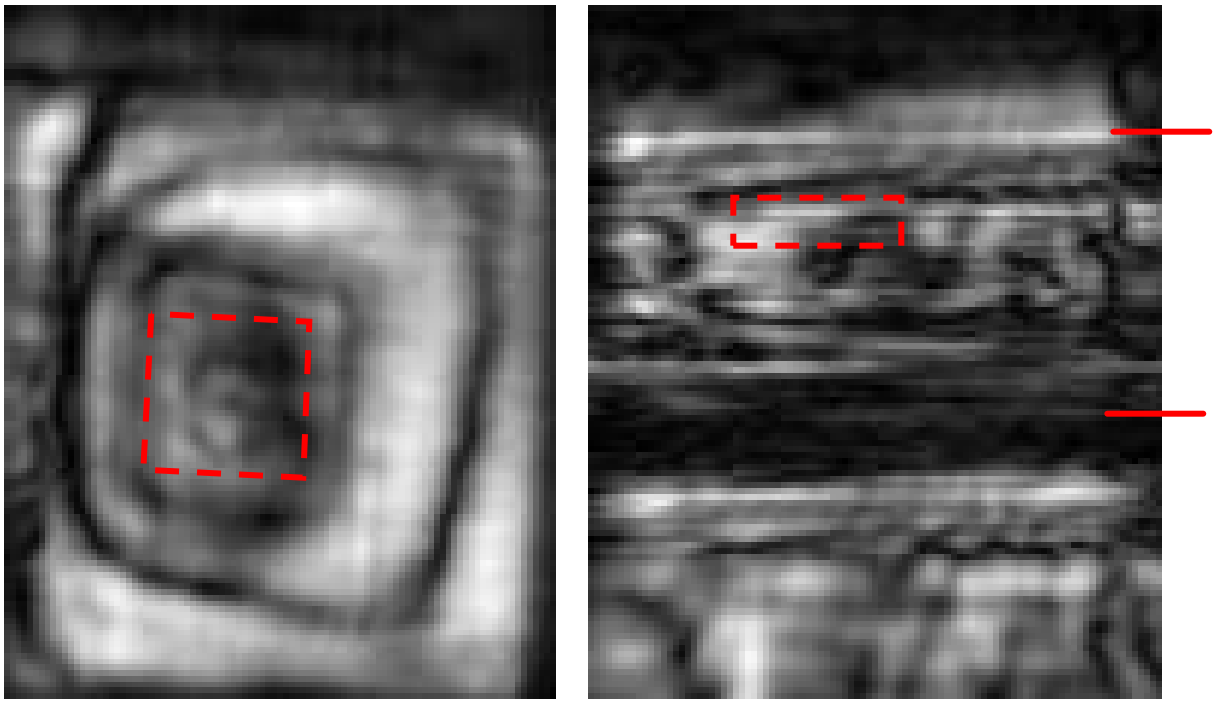

(a) **(b)**

Figure 11. PERES II results from a simulated concrete crack specimen with a minimized air gap. (a) Plan view image of reconstructed data (b) elevation view of reconstructed data.

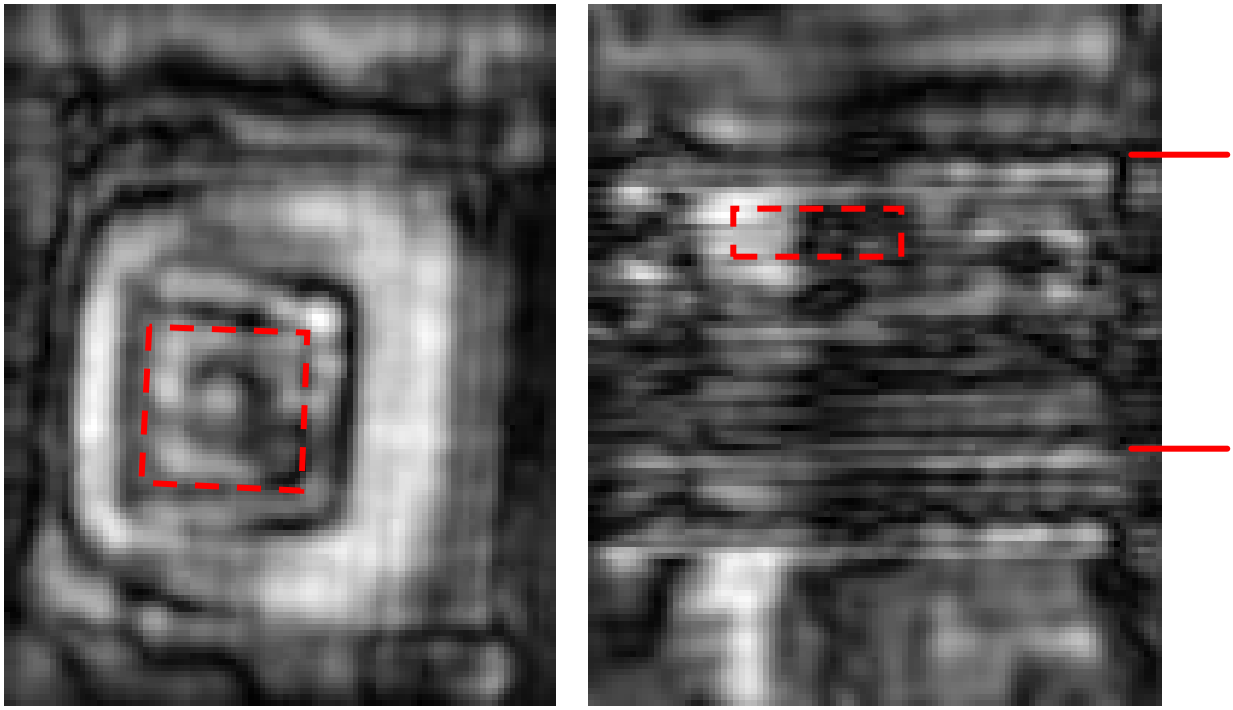

(a) **(b)**

Figure 12. PERES II results from a simulated concrete crack specimen with an approximate 0.25 cm air gap. (a) Plan view image of reconstructed data (b) elevation view of reconstructed data.

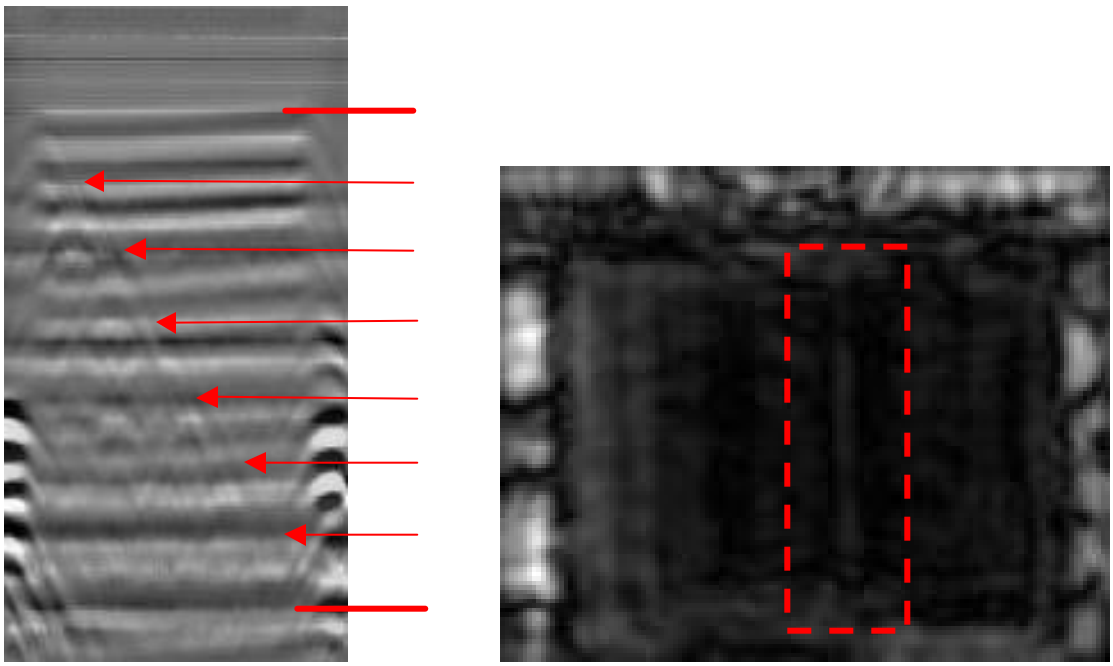

(a) **(b)**

Figure 13. Variable depth reinforcing steel specimen (a) raw PERES II response elevation view indicating six pieces of reinforcing steel, designated by arrows (b) reconstructed plan view response (9 cm depth) with a detected reinforcing steel bar enclosed by a dashed line box.

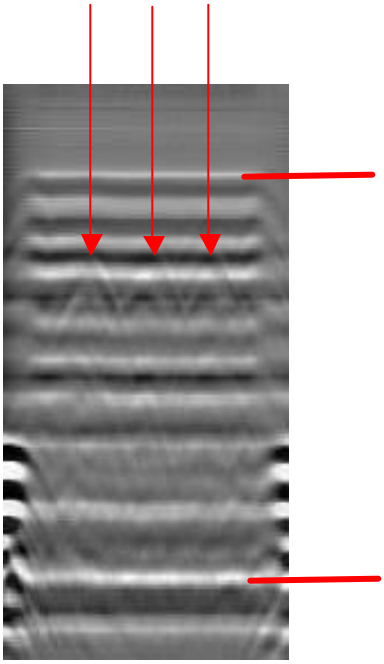

Figure 14. Raw PERES II elevation view response illustrating indications of variable diameter PVC pipe, designated by three vertical arrows.

Results from these specimens indicated an inconclusive sensitivity to variations in the diameter of voids and steel with variable sizes (based on PERES II results from specimens C4 and C5). Further study of these issues will be required to arrive at more conclusive findings.

5. Field Validation Testing

PERES II field validation testing was carried out at four different bridge decks. This testing was conducted in two phases, where the initial testing phase was conducted at the Van Buren Road Bridge and the subsequent phase was carried out at the Carter's Creek, Chatham and Lake Anna bridges. The initial testing phase allowed procedures and data analysis to be streamlined and improved before conducting tests at bridge decks with higher traffic volumes and other logistical demands. Ground truth data was collected from all of the bridge decks that were tested and this data was used in all cases to evaluate PERES II performance.

5.1 Initial testing at the Van Buren Road Bridge

Initial testing at the Van Buren Road Bridge was conducted on the north span and center span in the areas designated in Appendix D, (Figures D1, D2 and D3). PERES II data was collected on three different days to provide the best coverage of the deck possible and to refine the procedures used to conduct the testing. Two separate sounding surveys of the Van Buren Road bridge and coring of the bridge were all used to provide ground truth data for comparison to the PERES II data that was collected.

5.1.1 Description of the Van Buren Road Bridge

The Van Buren Road Bridge was built in 1963 and is comprised of three steel beam spans with a concrete bridge deck. The deck has a bare concrete surface and typically experiences low traffic volumes. The illustrations of the north and center spans in Figures D1, D2, and D3 show the bridge deck with a 1 ft grid added graphically to indicate the scale of collected bridge deck data and features. Each of the two illustrated spans is approximately 60 ft long.

5.1.2 Ground truth data

PERES II data was compared to ground truth data from the Van Buren bridge collected using three different methods. A hammer sounding test was conducted by two representatives from the New York Department of Transportation, NYDOT, along with a chain drag survey and coring conducted by staff from the NDEVC. The NYDOT hammer sounding survey was conducted by striking the bridge deck with a small hammer with a broad head and listening for either a solid or a hollow response. The delamination indications identified with this sounding test are illustrated with blue shaded areas on the bridge deck diagrams in Figures D1, D2 and D3 in Appendix D. These same diagrams also indicate delaminated areas detected using a chain drag survey as green shaded areas. This chain drag survey was conducted by listening for a solid or hollow sounding acoustic response to a chain dragged across the surface of the bridge deck. Cores on the two illustrated spans are also indicated on these diagrams. Table 1 provides results

Table 1. Van Buren Road Bridge coring results.

Core	Result
1	Delaminated
2	Delaminated
3	Solid
4	Solid
5	Solid
6	Delaminated
7	Delaminated
8	Solid
9	Delaminated
10	Solid

(a) (b)

Figure 15. (a) Core #8 (solid) and (b) core #6 (delaminated) from Van Buren Road Bridge.

from the cores, which agree with both the chain drag and the hammer sounding results. Examples of delaminated and solid cores from Van Buren Bridge are presented in Figure 15.

5.1.3 Summary of test results

The data in Figures D1, D2 and D3 illustrates typical responses from PERES II for three respective data sets. These data sets represent PERES II responses that will be recurring themes throughout the test results summaries. At the top of each figure, the bridge deck location corresponding to the PERES II data collection location is defined by a bold, red, dashed line. A scaled, straightened image of the data collection area and ground truth data is presented above the PERES II data for reference. The corresponding PERES II data from the area defined in the bridge diagram at the top of the page is then presented as a succession of progressively deeper tomographic image layers, typically referenced to a feature in the bridge deck.

The tomographic layers in Figure D1 range from the strip of data nearest the top of the page, corresponding to the radar response from the top surface of the bridge deck to the strip of data nearest the bottom of the page, corresponding to the bottom surface of the bridge deck. In this instance, both of these images contain distinctive features. The top surface radar response contains several sharp point reflections from small pieces of foil tape that were used as reference markers on the surface of the deck. In addition, some more broadly distributed variations in the surface reflection also appear where there may be some variability in either the surface properties or geometry. The bottom surface response includes a distinctive feature, indicative of a reflection from the flange of one of the steel beams that support the bridge. The feature is a dark

rectangular area in the data that extends from the bottom left of the image to just above the bottom right of the image. This is an important feature to note, since it indicates that the PERES II radar penetrated the full depth of this particular bridge deck. The geometry of the data collection relative to the bridge deck confirms that this feature corresponds to the location of one of the supporting bridge beams.

The middle two images, labeled as the top and bottom reinforcing steel mesh layers, illustrate typical PERES II responses to reinforcing steel. The top mesh clearly captures the skew of the reinforcing steel and the locations toward the bottom of the image where additional reinforcing steel appears. This additional steel reduces the spacing of the steel in the transverse direction to half that observed in the upper half of the image. This section of data does not present many opportunities for comparison to delaminated areas detected by sounding, and the areas that do offer a comparison between ground truth and PERES II data do not demonstrate an any significant correlation between them. However, it is significant that the reinforcing steel and solid concrete in this illustrated section is effectively imaged. The bottom reinforcing steel mesh is not clearly imaged, particularly relative to the top mesh.

Two additional data sections from the Van Buren Road Bridge are presented in Figures D2 and D3. These data sections were collected from two areas of the deck where both the NYDOT and NDEVC acoustic surveys determined that delaminations were present over a significant proportion of the tested area. In Figure D2, the top mesh of reinforcing steel does not indicate a correlation with the distress mapped by the acoustic surveys, but Figure D3 does display several features that are indicative of delamination detection. For example, in the lower left portion of the top mesh image in Figure D3, there are above average response values in the areas between the reinforcing steel mesh, indicating reflections from a feature in the concrete. In addition, the magnitude of the reinforcing steel reflection in this area of the image is reduced. This combination of effects is observed in delaminated areas in other collected data, as well, and will be described in more detail. Locally in this image, a similar effect can be observed up and to the right of the middle in the top mesh data on Figure D3, where another delaminated area appears to be observable in the PERES II data.

5.2 Bridge deck evaluation testing

The three bridges that were used in PERES II testing were briefly introduced in Section 1.5 as the Carter's Creek bridge deck, the Chatham bridge deck and the Lake Anna bridge deck. Each of these decks had specific characteristics that made it a good candidate for PERES II testing. The most important characteristic was that they each had significant known delaminated or deteriorated areas. In addition to the characteristics described in Section 1.5, coring activity had to be allowed and at least one of the tested decks needed to be an asphalt-overlaid deck. The following sections will describe the ground truth data and the PERES II results that were obtained for each bridge deck that was a part of the evaluation testing.

5.2.1 Carter's Creek Bridge deck

Carter's Creek Bridge has a bare concrete deck and consists of five spans, built using steel beam construction. The entire bridge is 288 ft in length and crosses Carter's Creek. This bridge deck has some delaminations, and many of these appear to have resulted in surface cracking. An illustration of a portion of Span 5 of Carter's Creek bridge deck is shown in Figure D4, which is relevant to the PERES II testing carried out at the bridge.

5.2.1.1 Ground Truth data

Ground truth data used to test for delaminations in Carter's Creek Bridge deck was collected by coring and chain drag testing conducted by NDEVC staff. This testing was conducted on the same day that PERES II testing was carried out at the bridge. Figure D4 illustrates the results from the ground truth testing at the Carter's Creek Bridge and indicates the locations of the cores that were extracted. Table 2 summarizes the results from the coring. Examples of solid and delaminated cores from Carter's Creek Bridge are presented in Figure 16. There are conflicting results between the chain drag testing and the coring results that should be noted. In particular, core 5 identifies a delamination that was not identified by the chain drag test. In addition, cores 6 and 3 were not delaminated even though the chain drag test indicated

Table 2. Carter's Creek Bridge coring results.

Core	Result
1	Solid
2	Solid
3	Solid
4	Solid
5	Delaminated
6	Solid
7	Solid

(a) (b)

Figure 16. (a) Core #5 (delaminated) and (b) core #2 (solid) from Carter's Creek Bridge.

that these areas were delaminated. These discrepancies could be related to the time limited constraints on the chain drag data collection for this particular test or simply related to some of the inconsistencies frequently observed in chain drag testing [9].

5.2.1.2 Summary of test results

The PERES II field test results for Carter's Creek Bridge Deck are presented in Figure D4. This data displays some interesting results, as well as a few that conflict. One certainty is that core 5 was delaminated when it was removed from the bridge deck. The corresponding return in the PERES II data is a diminished response in this area from the reinforcing steel. This diminished response relative to the surrounding response to reinforcing steel in the top mesh of

the PERES II data, (along with the corresponding reduced responses in the bottom mesh and bottom surface PERES II responses) are all clearly evident. In the image of the top mesh of reinforcing steel, there are also some small areas in the vicinity of core 5 that may correspond to an increase in the magnitude of the PERES II response, due to the presence of a delamination. In addition, there is a significant response to the apparent delamination detected by chain drag in the vicinity of core 6. Although core 6 was not delaminated, this general area was determined to contain delaminations using chain drag testing. The PERES II response in this area exhibits similar characteristics to those just discussed in reference to the area around core 5.

It is noteworthy that the two aforementioned responses, where delaminated areas are identified, are consistent with PERES II responses in areas where coring and chain drag results are in agreement. However, it should also be noted that several areas found to be delaminated using the chain drag test produced no variations in the PERES II data. A hypothesis has been developed to address these variations and is presented in Section 6.

5.2.2 Chatham bridge deck

The Chatham bridge deck was built in 1941 and consists of two curtain wall abutments, nine three-column piers and ten continuous steel beam spans that are 1005 ft in total length. The bridge has a concrete deck with an asphalt overlay and carries heavy traffic in the town of Fredericksburg, Virginia.

5.2.2.1 Ground truth data

Ground truth data for the Chatham bridge deck was only provided by results from coring, since an asphalt overlay precluded effective acoustic testing, such as chain drag testing, from being conducted. The results from this coring are provided in the Table 3 and images of cores are presented in Figure 17.

Table 3. Chatham bridge coring results.

Core	Result
1	Solid
2	Delaminated
3	Subsurface Concrete Patch
4	Subsurface Concrete Patch
5	Solid
6	Solid
7	Solid

(a) (b)

Figure 17. (a) Core #3 (concrete patch) and (b) core #1 (solid) from Chatham Bridge.

5.2.2.2 Summary of test results

PERES II test results from the Chatham Bridge indicate that PERES II can image basic bridge deck features effectively through asphalt, such as a concrete patch or reinforcing steel. The quality of the PERES II images is illustrated by data presented in Figure D5. Here, two relatively short sections of data are presented for review. Technical difficulties with PERES II precluded more data from being collected at this bridge. Even though a relatively short section of data was obtained from Chatham Bridge, some interesting results were produced. For example, cores 3 and 4 were both observed to contain concrete patch material, which appears to be indicated by an increased magnitude response in the lower left corner of the PERES II data,

(from the top reinforcing steel mesh) corresponding to these cores. In addition, the delamination observed in core 2 appears to correspond approximately to the location of an unusual loop shaped feature in the lower half of the top mesh data from PERES II corresponding to core 2. It is not clear if this is a coincidence or if these features are related.

5.2.3 Lake Anna bridge deck

The Lake Anna bridge deck is a curved steel bridge with a bare concrete bridge deck, built in 1970. This structure carries Route 208 traffic across Lake Anna, southwest of Fredericksburg and is approximately 928 ft long.

5.2.3.1 Ground truth data

Ground truth data was collected by coring and by a Virginia Department of Transportation (VDOT) chain drag survey of the Lake Anna bridge deck. Table 4 presents the results from the coring and Figure 18 provides photographs of two of the cores that were collected from the deck.

(a) (b)

Figure 18. (a) Core #1 (solid) and (b) core #9 (delaminated) from Lake Anna Bridge.

Table 4. Lake Anna bridge deck coring results.

Core	Result
1	Solid
2	Solid
3	Delaminated
4	Delaminated
5	Solid
6	Delaminated
7	Solid
8	Delaminated
9	Delaminated
10	Solid
11	Delaminated
12	Delaminated
13	Delaminated

5.2.3.2 Summary of test results

Several results from the data collected by PERES II at the Lake Anna Bridge indicate delaminations may have been imaged using PERES II. Figures D6, D7 and D8 all present results from two spans of this particular bridge deck. Figure D6 provides a very distinct image that appears to correspond to the shape of the VDOT chain drag mapping of the delaminations in this bridge deck, with a possible offset between the locations that could account for the discrepancies that appear between the PERES II image and the VDOT delamination survey. The features of interest in this image are the reduced magnitude response to the reinforcing steel along a curving boundary that divides the top and the bottom half of the top mesh reinforcing steel image. A similar boundary in the bottom mesh reinforcing steel image appears to result from a shadowing effect that may block the response to deeper features when a significant delamination crack is present. Applying an offset to the data collection location window moves it approximately 1.5 ft east and 1 ft north, which would also improve the agreement between coring results and the chain drag survey substantially. If these adjustments are valid, which is plausible since only

basic measurement techniques were applied on a curved bridge, then the two results can be aligned substantially on top of one another. The results in Figures D7 and D8 also indicate that delaminations, which cover the entire area beneath both of these scans, may have been imaged in a similar fashion.

6. Discussion and Findings

Results from PERES II testing indicate that the system has significant concrete bridge deck evaluation capabilities that advance the state of the art in GPR applications to bridges. Specifically, the PERES II system is the first GPR FHWA is aware of that appears to be capable of directly imaging concrete bridge deck delaminations in verified locations in a field bridge deck. The following sections evaluate several areas of system performance in both laboratory and field tests. The evaluation criteria set out by HERMES II project pooled fund states in Section 1.3 are also discussed. In Section 6.4, the performance of the system relative to these criteria is summarized based on field test results and an initial interpretation of these results. Because PERES II is a prototype system, it should be noted that these results remain preliminary and advances in the interpretation and understanding of the results the system produces remain a possibility.

6.1 Discussion of laboratory tests

Laboratory testing of PERES II revealed two important findings and indicated the need for further investigation in other areas. One of the key findings was that air gaps between parallel plates and simulated cracks were detectable, down to currently simulated size range of several millimeters. Previously observed trends in radar responses, such as the reduction in the magnitude of the radar response with decreasing air gap size were confirmed to hold for PERES II results, as well. The other key finding was that the geometry of the crack relative to the bridge deck surface affected whether it was imaged by the system. Crack areas at oblique angles, particularly if they exhibit a rough textured surface morphology, are not as likely to be imaged as orthogonal planar surfaces. All of these results informed the interpretation of field test results

and underpinned the findings from them. The penetration depth that the system can achieve was quantified as a minimum of 18 cm in the laboratory and this finding was confirmed by imaging the flange of a steel beam below the surface of an 18 cm thick bridge deck during field-testing. Areas that were determined to require further investigation included sensitivity to the size and geometry of reinforcing steel and voids.

6.2 Discussion of field tests

PERES II field tests carried out during this study have produced significant results for GPR applications to bridge decks. These results, presented in Section 5, indicate that delamination cracks in concrete bridge decks can be imaged by PERES II. However, these cracks only appear to be imaged when they reach a threshold size, as measured through the depth dimension of the deck. This threshold size is not fixed, since many variables affect it, but it appears that many of the delaminations that were encountered in field testing were within detectable limits. The concept of this detected crack size threshold and its impact on the PERES II response to delamination cracking, continues to be an important finding. This concept is based on the hypothesis that radar resolution and delamination crack detection are related for GPR applications to bridge decks and is supported by results from laboratory testing and radar theory [10]. A summary table of the areas covered by the field test surveys, providing details regarding the total area surveyed and the delaminated area detected is provided for all of the test bridges in Appendix E, (Tables 1 and 2).

6.3 Assessment of system functionality

The basic functionality of PERES II was tested both in the laboratory and the field to provide an assessment of the viability of deploying similar instruments for regular use under demanding field conditions. For a significant proportion of the testing the system performed well and allowed data to be collected efficiently. However, there were some significant problems that occurred during testing that caused delays and even required one test to be completely aborted. The typical operation of the system will be discussed in this section

along with the problems, troubleshooting and eventual resolution of issues related to individual system failures.

The PERES II design requires several software and hardware components to work in concert with one another during system calibration and data collection. These software and hardware components and many details of system function are described in detail in Section 2.1.3. Briefly, PERES II has a motion control system that moves the antenna to precise positions above a given bridge deck while radar and data acquisition equipment collect SAR data and store it digitally for later processing. All of these functions are controlled by the on-board PERES II computer. With these functional elements working together, the operation of the system is typically smooth and precise. Physically the system moves to user-designated positions in specified increments. The user interface and computer software make controlling the physical functions of the system relatively intuitive.

Data collection, which requires a radar pulse to be transmitted, received and subsequently digitized by an analog to digital converter, is reliable and predictable. Adjustments and calibrations are required to account for any variability that occurs due to temperature or other environmental factors that affect the system. These calibration functions have been refined to work smoothly, even under difficult field conditions. Post-processing techniques have been developed by LLNL to handle most problems that can occur during analog to digital conversion or due to signal clutter.

Data was collected and system calibrations were carried out without any malfunctions during three separate trips to the Van Buren Road Bridge. These three trips were planned to maximize the data collection coverage area on this bridge deck and to concurrently refine field logistics. After these three successful trips, plans for the first field test to be conducted by FHWA NDE Validation Center staff at a bridge requiring traffic control logistics were finalized. The Lake Anna Bridge deck was selected and used for this test.

Immediately after deploying PERES II on this bridge deck, the PERES II motion control system failed to function. A range of troubleshooting steps were taken in an effort to remedy this situation, after examining the feedback the system provided, including substituting spare stepper and servo motors into the system and substituting spare motor driver components. After these substitutions failed to improve the situation, the suspected problems with the system narrowed to either the system "master controller," (a device that provides an interface between the PERES II

computer and the servo motor drivers) or a computer related problem, such as a corrupted file. The spare PERES II master controller was examined and it was quickly determined that it was not identical to the currently installed master controller. Knowing that the master controller might have been the cause of the problem and that the computer problem could be more effectively addressed back at the NDEVC, a decision was made to return to the lab and systematically troubleshoot the system.

Troubleshooting in the laboratory revealed that replacing the system hard drive with a mirror copy of the original hard drive brought the system back up properly and got the motion control aspect of the system running again. After this was successfully accomplished, the system was run for approximately an hour to make sure it was ready to return to the field. The system was then packed up and made ready for a test on the Chatham Bridge in Fredericksburg.

Testing at the Chatham Bridge proceeded normally, initially, as data was collected along a 6.5 m length of the deck. However, during data collection, the system abruptly stopped functioning. Again, troubleshooting steps were taken in the field, but the problem was not diagnosable in the limited time remaining to test at the Chatham bridge deck. Because it was an extremely hot day (over 100 degrees Fahrenheit) and the servo motors had become hot to the touch relative to their typical operating temperature, the system problem appeared to be related to an overheating issue. The additional fact that the system worked again after it was reassembled, in the relatively cool laboratory environment several hours later, made this theory even more plausible.

Ongoing discussions with LLNL were continued to ensure a correct diagnosis of the problem was made. Eventually, a related hypothesis for the root cause of the problem was developed. After additional factors had been considered, the spare servo motor driver that LLNL had provided was found to have programmed constants that were not fully compatible with the motion control constants for PERES II. The default constants programmed into this spare servo motor driver had allowed the system to run for several hours, but eventually the difference between these default parameters and the correct system parameters caused the servo motors to heat up. Eventually a temperature limit switch in the servo motor was tripped and the system automatically shut down. The final solution was to reprogram the spare servo motor controller, (which had been installed during troubleshooting at the Lake Anna Bridge) with appropriate

constants and subsequently run the system normally. After this issue was resolved, no further motion control problems were encountered during subsequent field and laboratory testing.

Ultimately, the design of the PERES II system proved to be functional and generally reliable for field use. Of the two problems the system exhibited during testing, one was caused by a corrupted hard drive and the other was caused by an improperly configured spare part. For a complicated system prototype, such as PERES II, some problems of this nature can occur in spite of a good system design.

6.4 Assessment of system performance relative to evaluation criteria

An initial assessment of PERES II shows that it does not meet the criteria set out in Section 1.3. This result is an important finding, but the context of this result should be considered. This study indicates that delaminations have been imaged by PERES II in field bridge decks, which this is the first time that a direct image of this type of feature has been verifiably achieved in the field, to the knowledge of FHWA. A conservative estimate indicates that PERES II imaged approximately 70 percent of the delaminations observed by the chain drag test in the most successful PERES II field results from the Lake Anna Bridge Deck. The first criteria set out in Section 1.3 was a tolerance for detecting delaminations that required a reliability of 90 percent through asphalt and concrete overlays, which is clearly not met by even the best performance of PERES II. The second was that PERES II should image delaminations through asphalt overlays. PERES II did not effectively image delaminations through an asphalt overlay, but it did image features such as a concrete patch below a thick asphalt overlay. Finally, the third PERES II evaluation criteria set out in Section 1.3 demanded that PERES II be capable of imaging bridge deck defects at the bottom level of the reinforcing steel in a concrete bridge deck. Although direct imaging of defects at this level was not confirmed during this testing, results from the field and the lab show that features such as reinforcing steel and material boundaries are imaged by the system at this level. Overall, the PERES II system has achieved a significant goal of imaging confirmed delaminated areas in bridge decks, but it has not achieved the larger goal of imaging these delamination features at a level that satisfies criteria set out at the inception of this study.

Appendix A

Data Processing Definitions:

Cleaned – A background signal obtained during testing is subtracted from the data.
Initial Parameters – Dielectric properties estimated based on the best available information from bridge deck cores or bridge plans are used as input to the wavefield backpropagation model.
Average Subtracted – The average response from the bridge deck is subtracted from all waveforms to minimize the effects of the surface reflection and signal ringing.
Unfolded – The digital gain profile originally applied to the data during collection is divided out of the response, leaving the originally collected signal.
Final Parameters – Dielectric properties are optimimized for the wavefield backpropagation model using an iterative optimization algorithm.

Appendix B

Virginia Department of Transportation A4 Concrete mix design.

Component	**Composition (kg/m^3)**
Cement	272
Slag	147
Fine Aggregate	845
Course Aggregate	907
Air Entraining Admixture	0.4
Water Reducer	0.8
Water	140
High Range Water Reducing Agent	2.1
Slump	72 mm

Appendix C

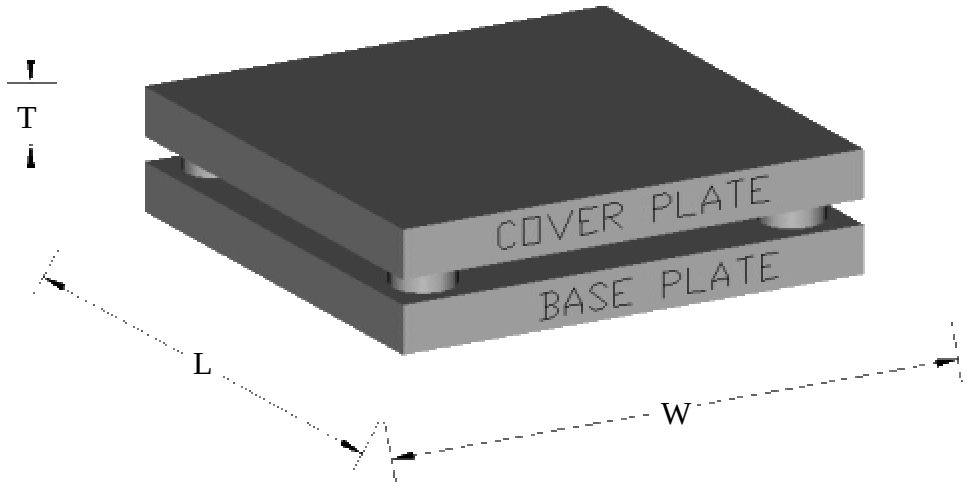

Figure C1. Parallel plate specimen design.

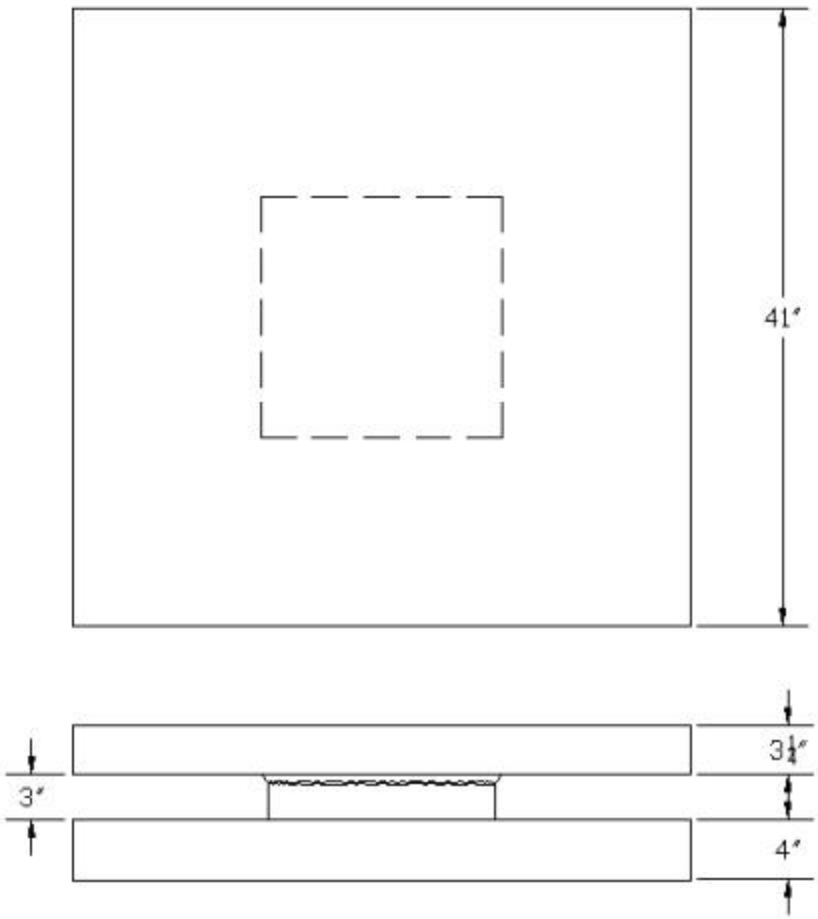

Figure C2. Simulated crack specimen.

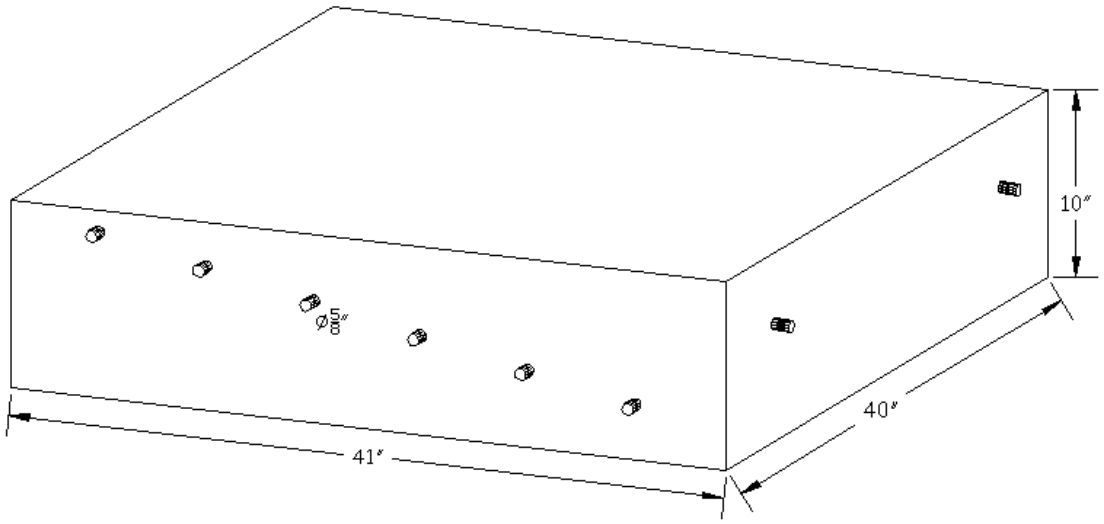

Figure C3. Variable depth reinforcing steel specimen.

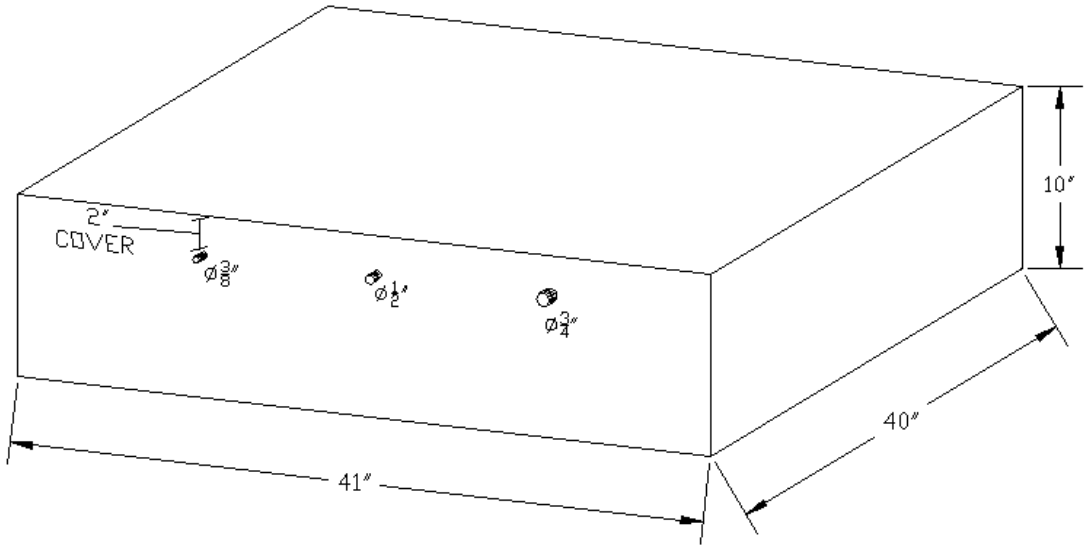

Figure C4. Variable diameter reinforcing steel specimen

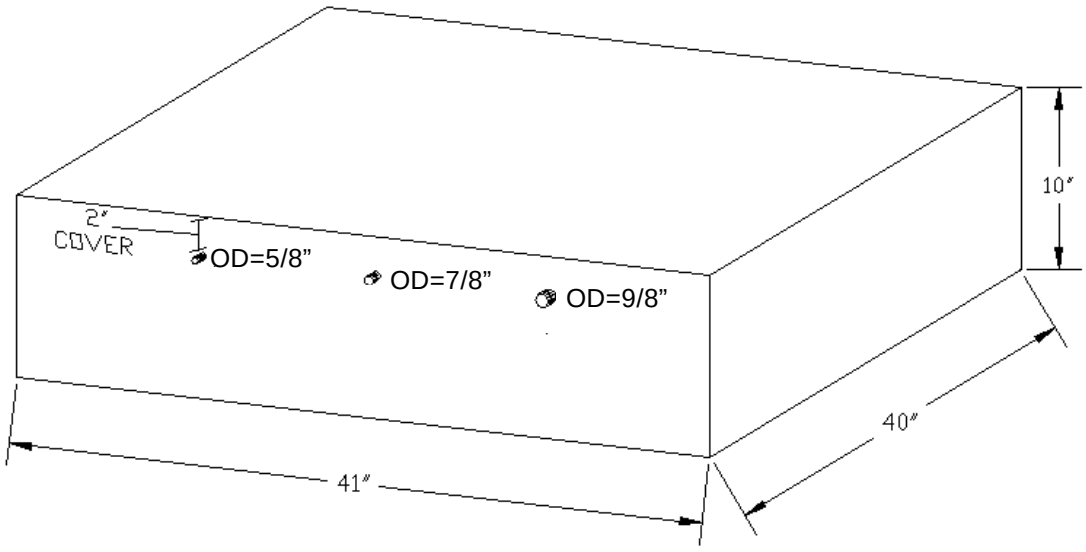

Figure C5. Variable diameter void simulation specimen.

Appendix D

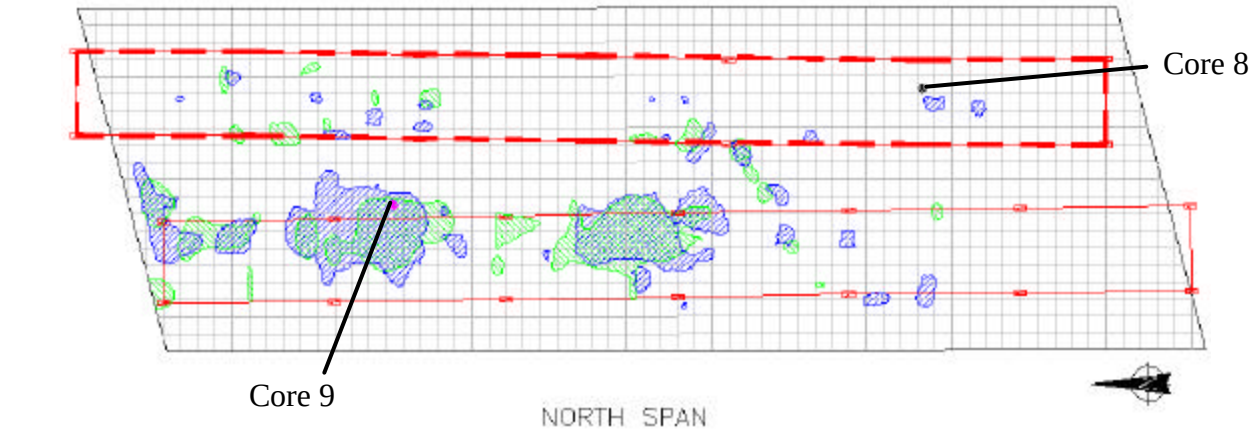

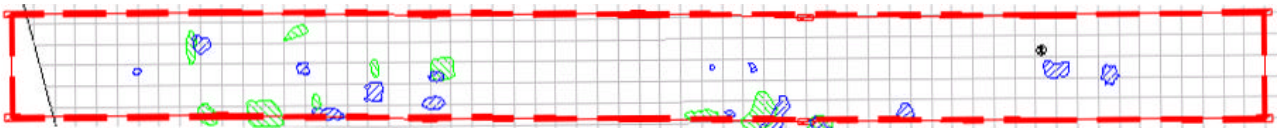

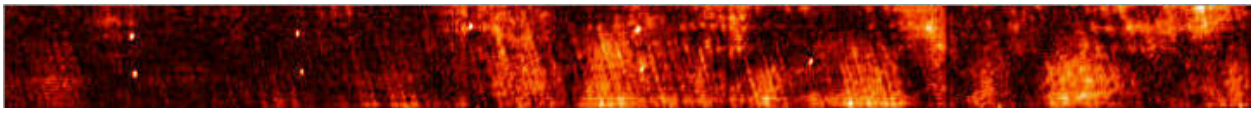

TOP SURFACE

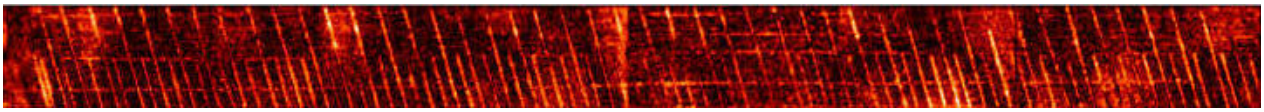

TOP MESH

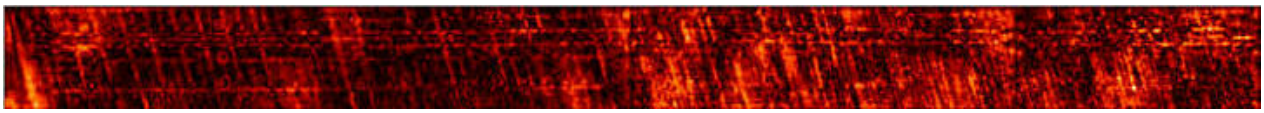

BOTTOM MESH

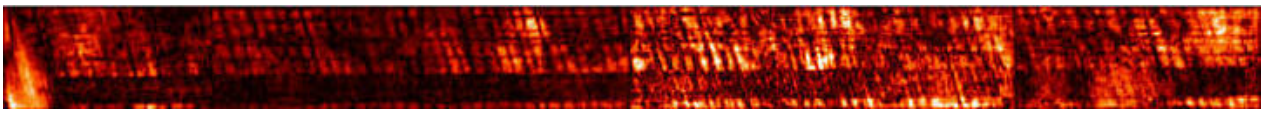

BOTTOM SURFACE

Figure D1. Van Buren Bridge north span, north bound data.

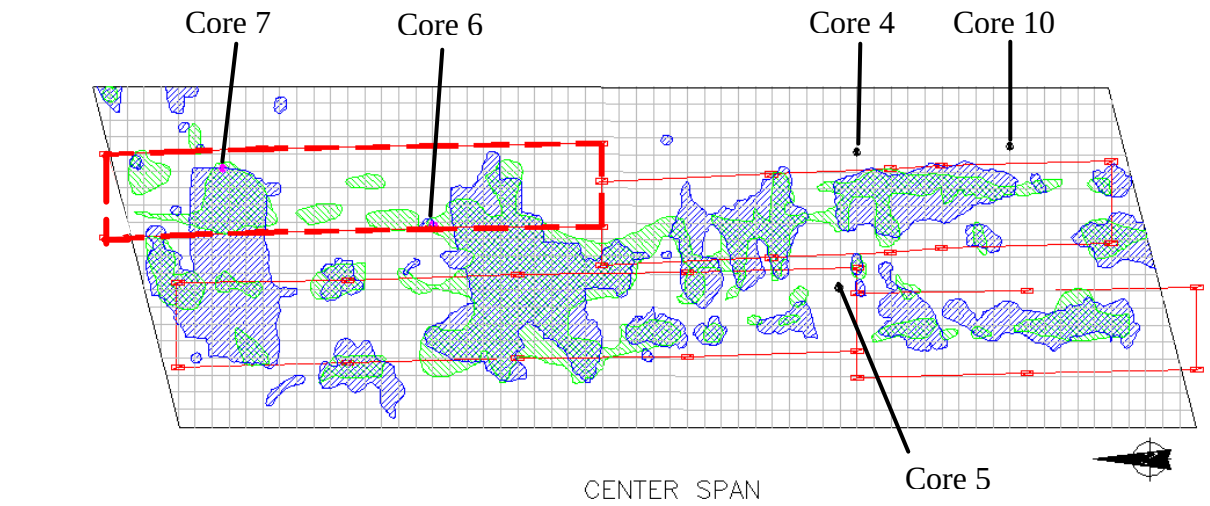

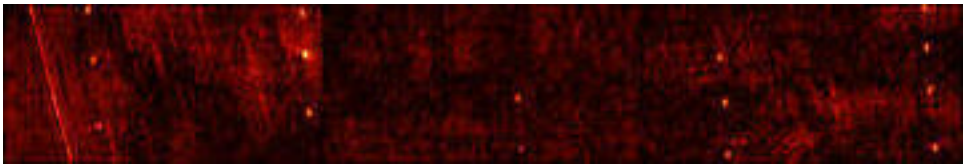

TOP SURFACE

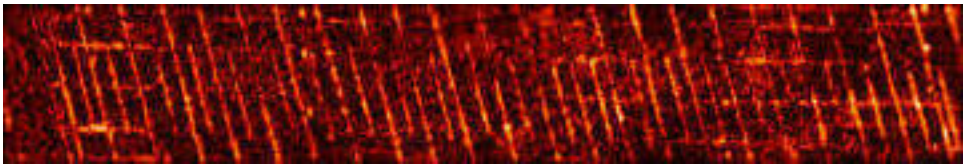

TOP MESH

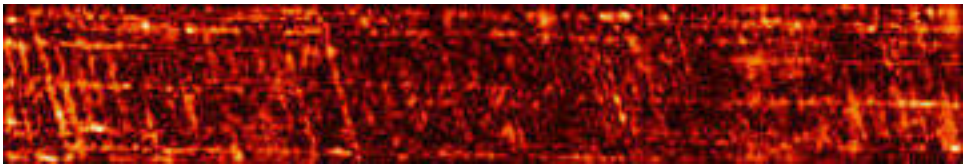

BOTTOM MESH

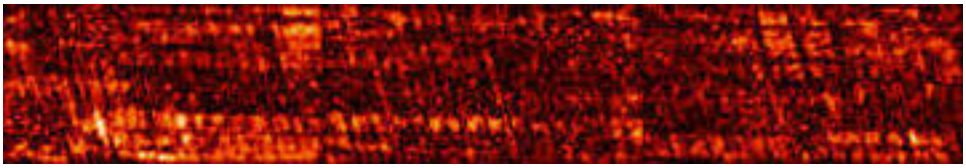

BOTTOM SURFACE

Figure D2. Van Buren Bridge center span, north bound data set 1.

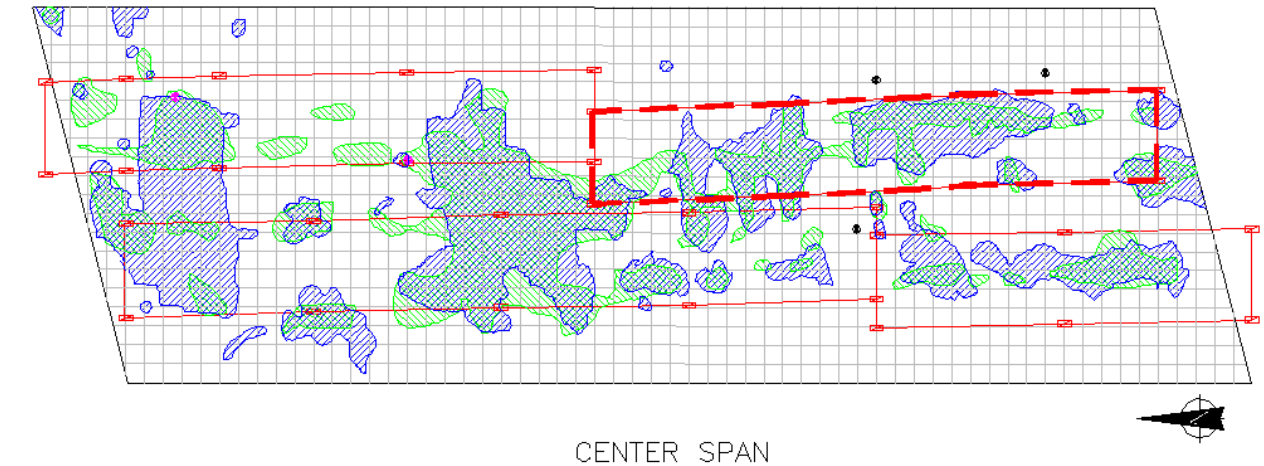

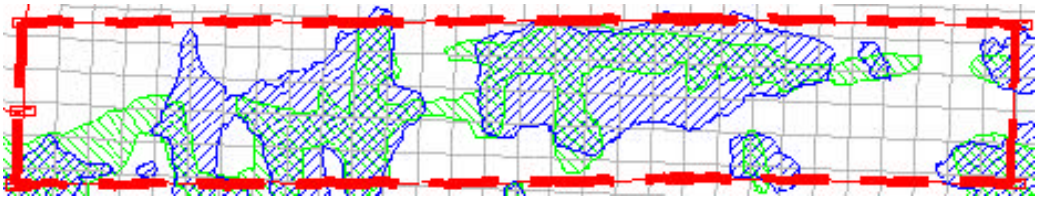

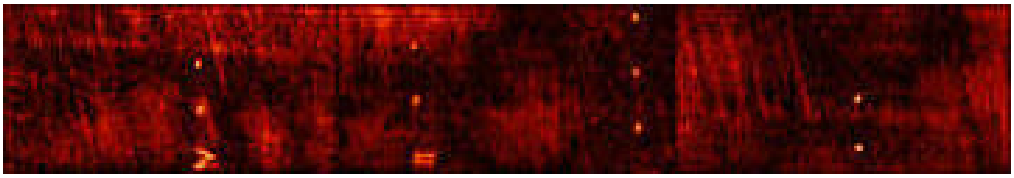

TOP SURFACE

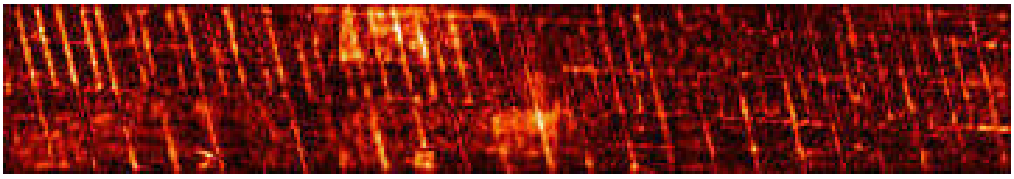

TOP MESH

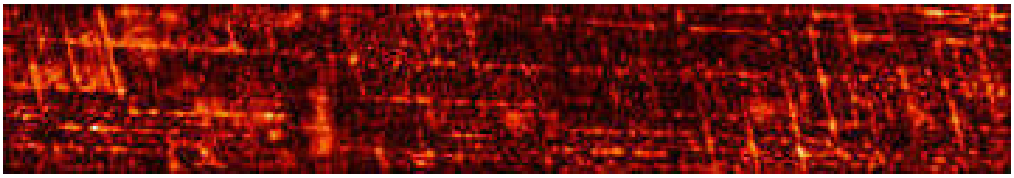

BOTTOM MESH

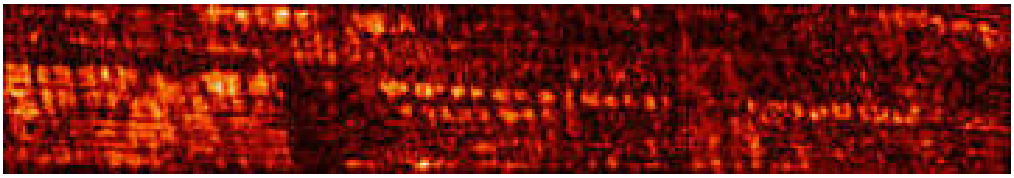

BOTTOM SURFACE

Figure D3. Van Buren Bridge center span, north bound data set 2.

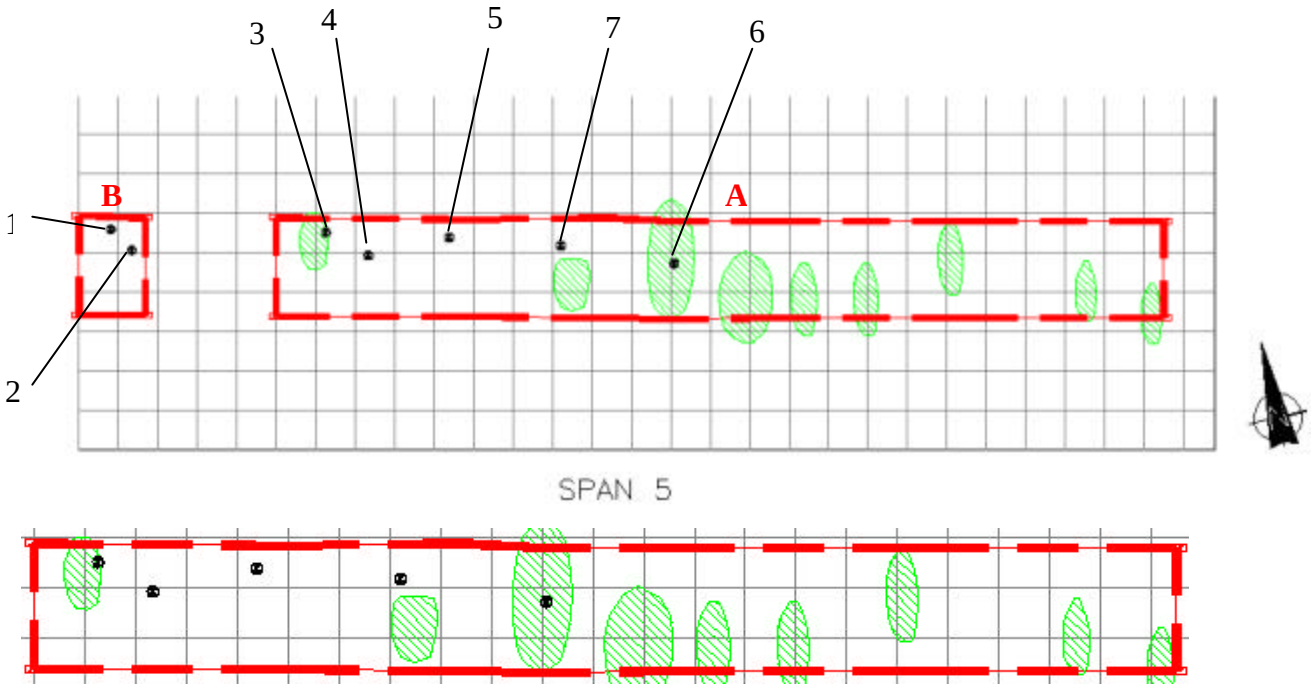

A

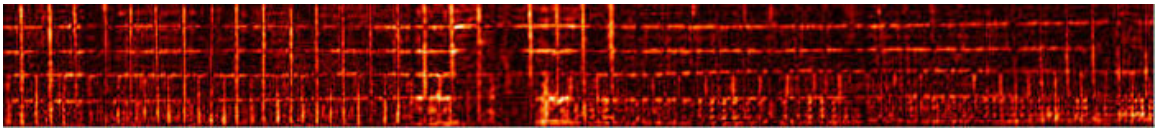

TOP MESH

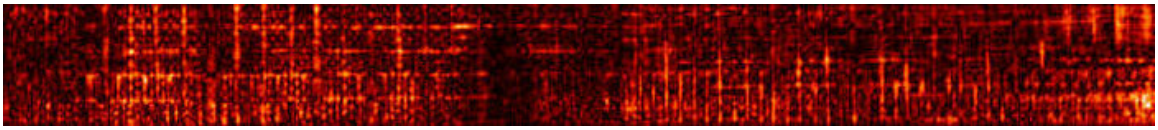

BOTTOM MESH

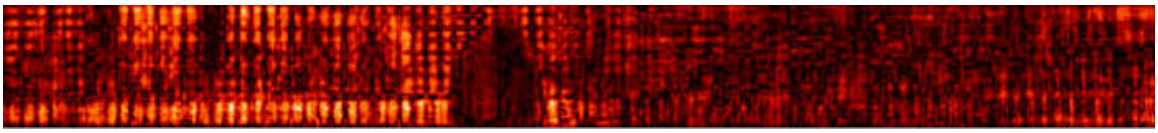

BOTTOM SURFACE

B

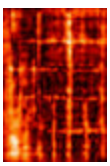

TOP MESH

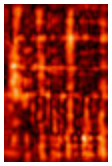

BOTTOM MESH

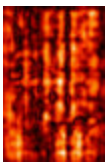

BOTTOM SURFACE

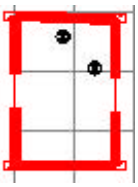

Figure D4. Carters Creek Bridge, span 5, east bound data.

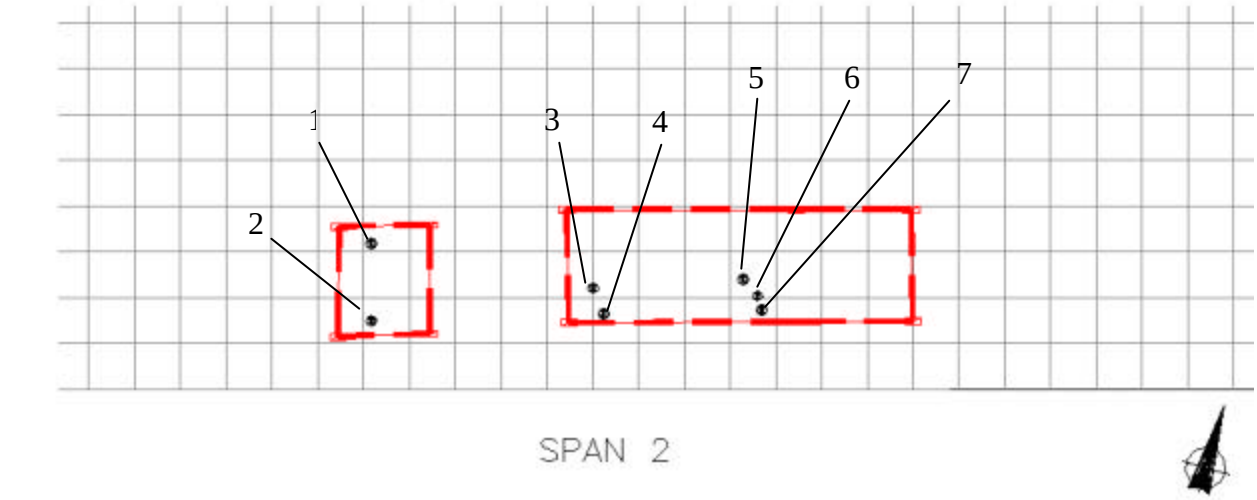

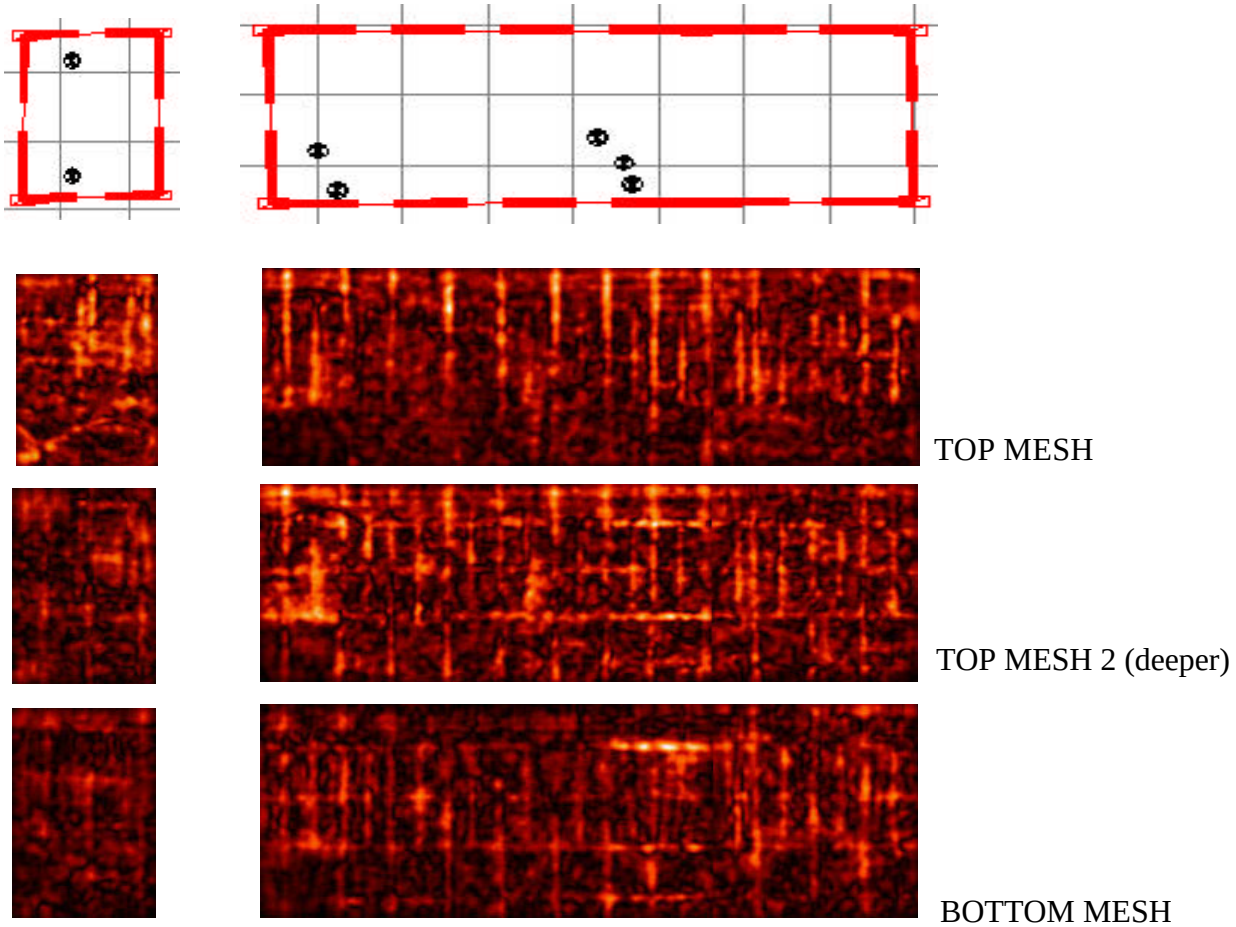

Figure D5. Chatham Bridge, span 2, east bound data.

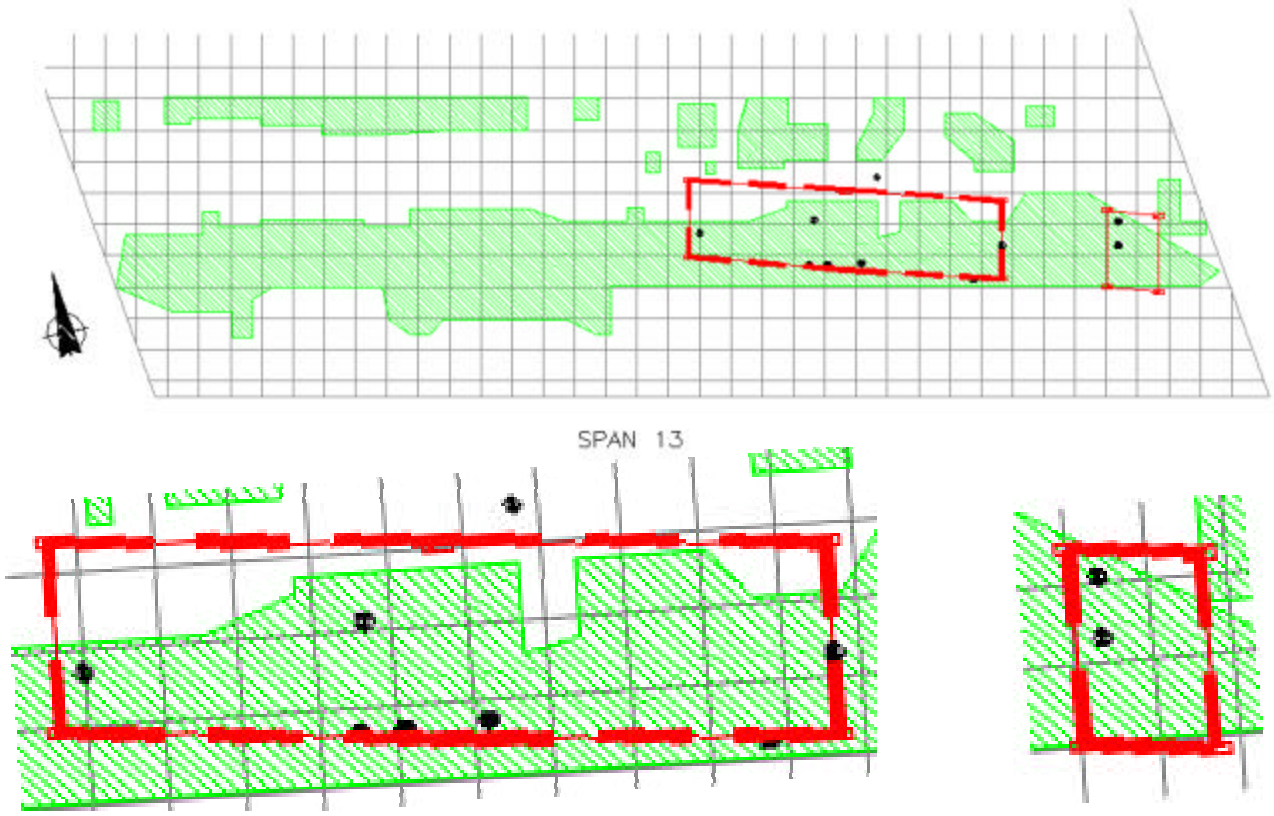

Figure D6. Lake Anna bridge, span 13, east bound data

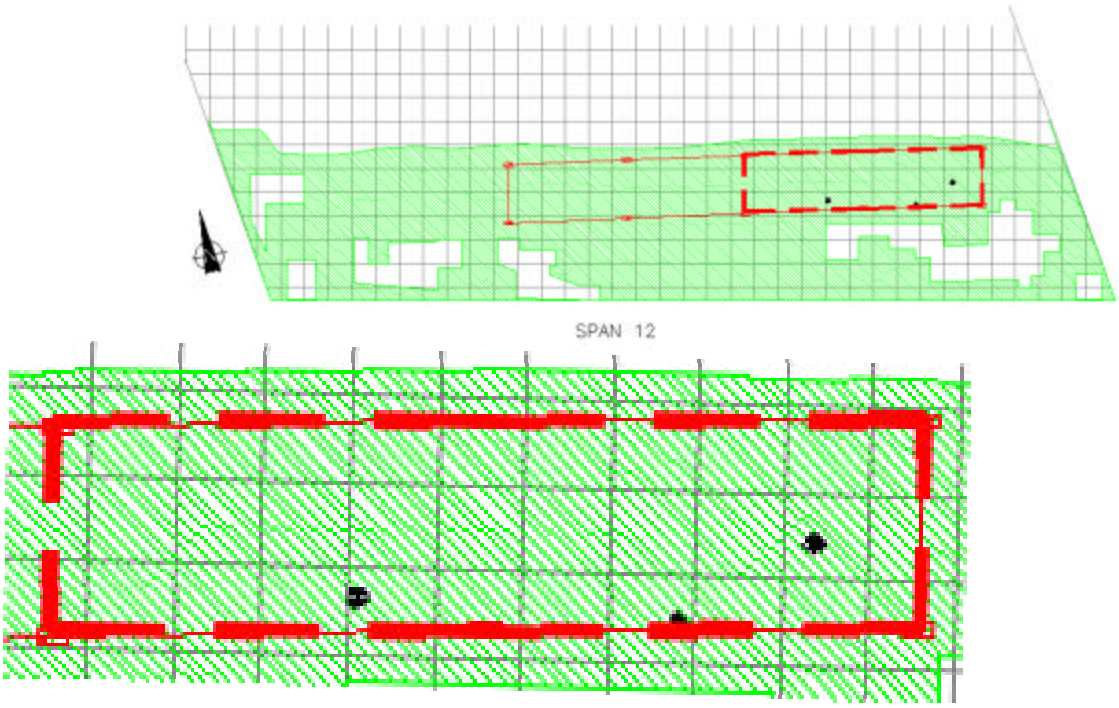

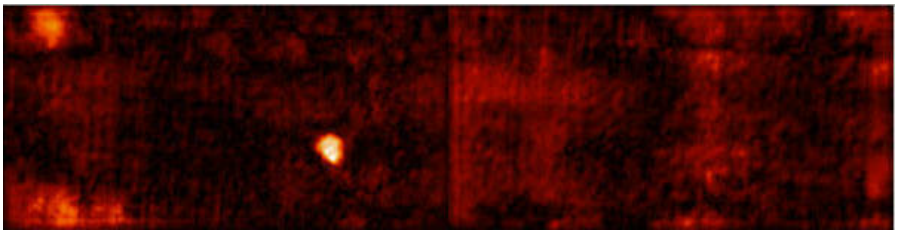

TOP SURFACE

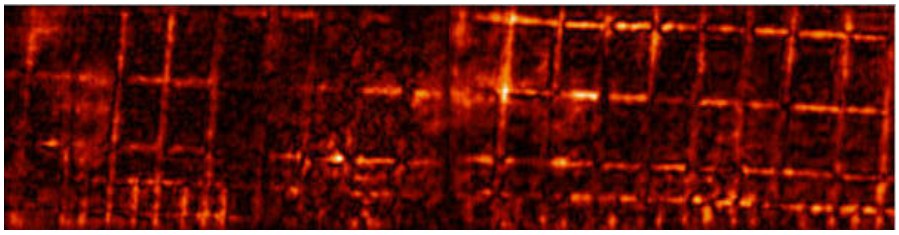

TOP MESH

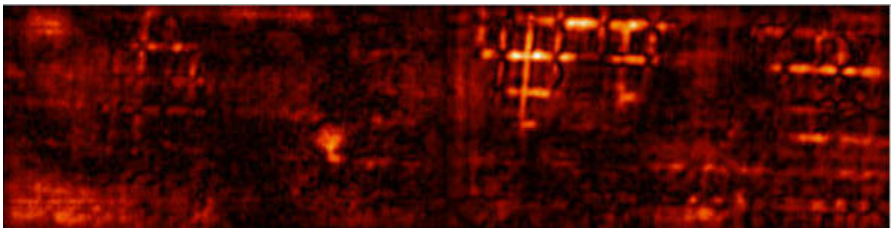

BOTTOM MESH

Figure D7. Lake Anna bridge, span 12, east bound data.

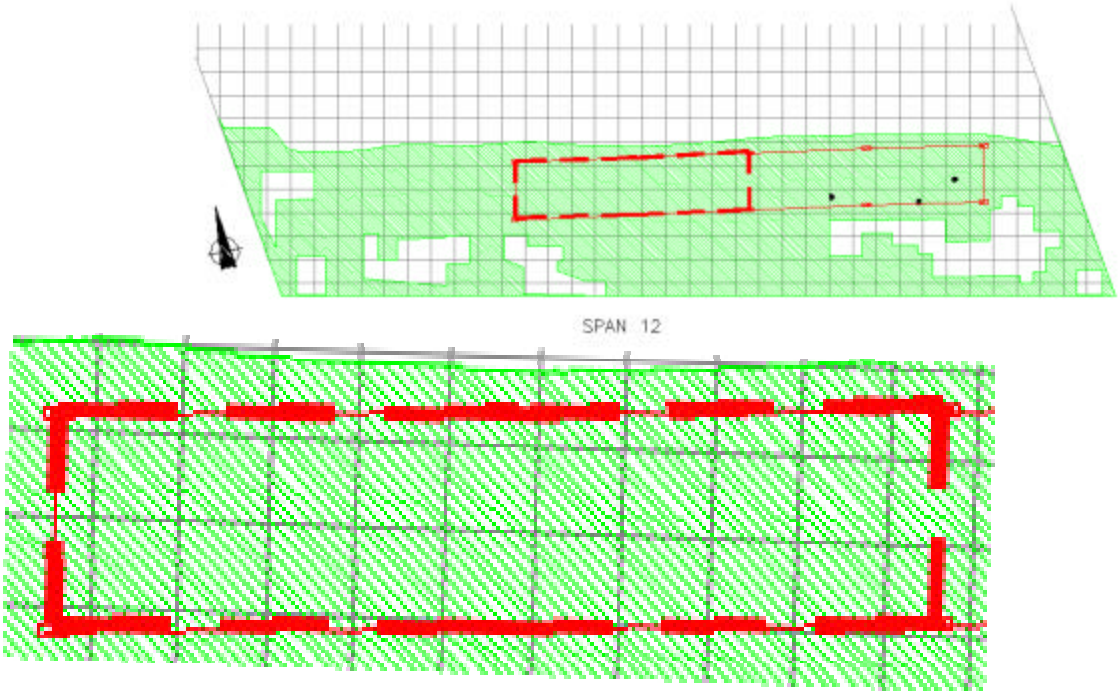

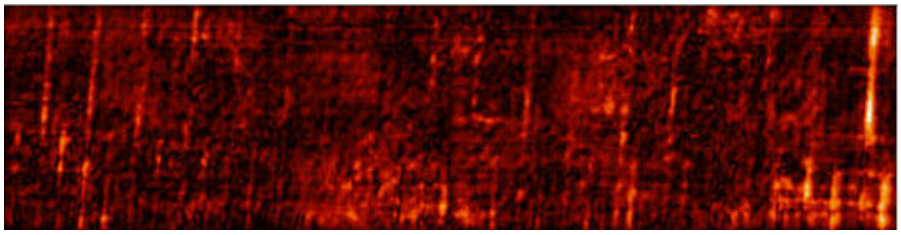

TOP SURFACE

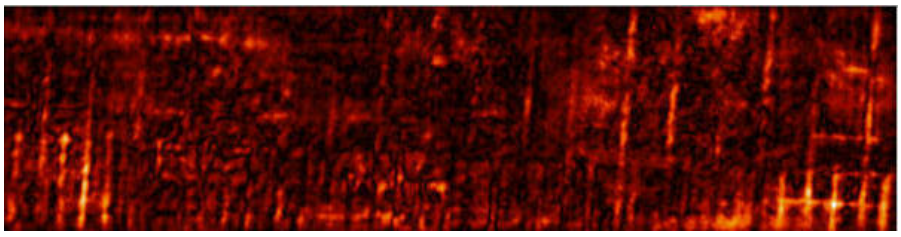

TOP MESH

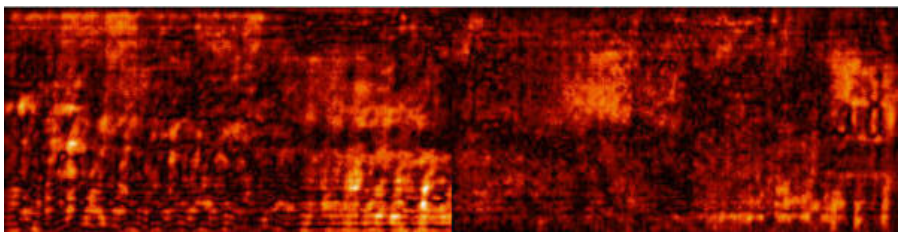

BOTTOM MESH

Figure D8. Lake Anna bridge, span 12, east bound data.

APPENDIX E

Table E1. Delaminated areas detected by each respective method and total survey areas covered (square feet).

Method	Van Buren	Carter's Creek	Lake Anna	Chatham
Radar	27	13	185	0
VDOT Chain Drag	NA	NA	272	NA
NYDOT Hammer Sounding	80	NA	NA	NA
NDEVC Chain Drag	64	9	NA	NA
Total Area Surveyed	600	240	315	90

Table E2. Delaminated areas detected by each respective method and total survey areas covered (square meters).

Method	Van Buren	Carter's Creek	Lake Anna	Chatham
Radar	2.51	1.21	17.19	0
VDOT Chain Drag	NA	NA	25.27	NA
NYDOT Hammer Sounding	7.43	NA	NA	NA
NDEVC Chain Drag	5.95	0.84	NA	NA
Total Area Surveyed	55.74	22.30	29.26	8.36

Bibliography

1. Scott, M., Rezaizadeh, A., Moore, M., "A Comparison of Nondestructive Evaluation Methods for Bridge Deck Evaluation," Scott, M., Rezaizadeh, A., Delahaza, A., Moore, M., Graybeal, B., Washer, G., Proceedings of Structural Faults and Repair, London, England, July 2001, pp. 14.

2. Scott, M., Duke, J., Davidson, N., Washer, G., Weyers, R., "Automated Characterization of Bridge Deck Distress Using Pattern Recognition Analysis of Ground Penetrating Radar Data," Materials Evaluation, Vol. 58, No. 11, November 2000, pp. 1305-1309.

3. Scott, M., Rezaizadeh, A., Moore, M., "Phenomenology Study of HERMES Ground Penetrating Radar Technology for Detection and Identification of Common Bridge Deck Features," Federal Highway Administration Report FHWA-RD-01-090, June 2001, pp. 27.

4. Federal Highway Administration NDE Validation Center Internal Test and Evaluation Report: "Testing and Evaluation of the HERMES Bridge Inspector", Project DTFH61-C-98-00050, January 3, 2000, pp. 69.

5. Davidson, N., Chase, S., "Radar Tomography of Bridge Decks," Structural Materials Technology III – an NDT Conference, SPIE Vol. 3400, San Antonio, Tx., March 31 – April 1, 1998, pp. 250-256.

6. Skolnik, M.I., Introduction to Radar Systems, McGraw Hill, Boston, Massachusetts, 1980, pp. 581.

7. Daniels, D.J., Surface Penetrating Radar, The Institution of Electrical Engineers, Short Run Press, England, 1996, pp. 300.

8. Mast, J.E., "Microwave Pulse-Echo Radar Imaging for the Nondestructive Evaluation of Civil Structures," Ph.D. Dissertation, University of Illinois at Urbana-Champaign, Urbana, IL, 1993, pp. 104.

9. Moore, M., Phares, B., Graybeal, B., Rolander, D., Washer, G., Reliability of Visual Inspection for Highway Bridges, FHWA-RD-01-020, June 2001, pp. 516.

10. Rihaczek, A.W., Hershkowitz, S.J., "Radar Resolution and Complex Image Analysis," Artech House, Boston, 1996, pp. 524.